

Sahas Bikram Shah

Finite Element Modeling of Losses due to Inter-laminar Short-circuit Currents in Electrical Machines

School of Electrical Engineering

Thesis submitted for examination for the degree of Master of Science in Technology.

Espoo 28.1.2013

Thesis supervisor:

Prof. Antero Arkkio

Thesis instructor:

D.Sc. (Tech.) Paavo Rasilo

Author: Sahas Bikram Shah

Title: Finite Element Modeling of Losses due to Inter-laminar Short-circuit
Currents in Electrical Machines

Date: 28.1.2013

Language: English

Number of pages:6+43

Department of Electrical Engineering

Professorship: Electromechanics

Code: S-17

Supervisor: Prof. Antero Arkkio

Instructor: D.Sc. (Tech.) Paavo Rasilo

Identification and accurate prediction of losses in electrical machines is very essential in design stage to minimize the cost and optimize the efficiency. The losses introduced in electrical machines due to manufacturing effects are significant. Burr formed due to punching on the edges of laminated sheets impairs the insulation of adjacent sheets and makes random galvanic contacts during the pressing of stacked sheets. The existence of a surface current on the boundary between two insulated regions causes discontinuity of the tangential component of the magnetic field strength. Hence, based on this principle, a boundary layer model was developed to study the additional losses on the burred edges of electrical sheets. The boundary layer model was then coupled with 2-D finite element analysis and incorporated into an inhouse FEM software to study the additional losses in a 37 kW induction machine.

Keywords: additional losses, burr, eddy currents, electrical sheets, finite element method, induction machine, Maxwell's equations, punching effect, UI sheet

Preface

This master thesis was carried out in Electromechanics research group at School of Electrical Engineering Aalto University. This research work is the part of the research programme *Future Combustion Engine Power Plants (FCEP)* and I would like to thank *CLEEN Oy* for their financial support.

First and foremost, I would like to express my deep gratitude to my supervisor Prof. Antero Arkkio and my instructor Dr. Paavo Rasilo for their patient guidance, enthusiastic encouragement and useful discussion. I would also like to appreciate the encouragement of Adj. Prof. Anouar Belahcen during my research work and I am also thankful to our Head of Department Prof. Asko Niemenmaa for providing good research environment.

Besides, I would like to thank Mr. Ari Haavisto for his technical assistance. I am also thankful to all my colleagues in Electromechanics research group for creating pleasant working environment. I am thankful to Bishal Silwal for helping me to proof read my thesis, Deepak Singh, Daniel Iruikwu, Jonanthan Velasco and Javier Martinez for productive coffee break discussions which helped me a lot during my research.

Last but not least, I would like to express my heartfelt thanks to my parents and sister for their ceaseless blessing, love and support. I would also like to thank all my friends, relatives and Aalto Nepali community for being there through thick and thin.

Otaniemi, 28.1.2013

Sahas Bikram Shah

Contents

| | |
|---|------------|
| Abstract | ii |
| Preface | iii |
| Contents | iv |
| Symbols and abbreviations | v |
| 1 Introduction | 1 |
| 1.1 Background | 1 |
| 1.2 Aim of thesis | 2 |
| 1.3 Outline of thesis | 2 |
| 2 Losses in sheets | 3 |
| 2.1 Iron losses | 3 |
| 2.2 Interlaminar faults | 5 |
| 2.3 Burr formation | 6 |
| 2.4 Literature review: Modeling formulations | 9 |
| 3 Methodology | 14 |
| 3.1 Finite element method | 14 |
| 3.1.1 Space discretization | 15 |
| 3.1.2 Time discretization | 16 |
| 3.1.3 Non-linearity | 16 |
| 3.2 Eddy current formulation | 17 |
| 3.3 Boundary layer formulation | 19 |
| 3.4 Model Analysis | 24 |
| 3.5 Computation algorithm and incorporation in FCSMEK | 27 |
| 3.5.1 Boundary identification | 28 |
| 3.5.2 Incorporation in FCSMEK | 28 |
| 3.5.3 Numerical integration | 30 |
| 4 Results and discussion | 31 |
| 4.1 Boundary layer model implementation in UI sheets | 31 |
| 4.2 Model application in cage induction machine | 35 |
| 5 Conclusion | 38 |
| References | 39 |
| APPENDIX A | 42 |
| APPENDIX B | 43 |

Symbols and abbreviations

Symbols

| | |
|------------------|---|
| \mathbf{a} | nodal values of the magnetic vector potential (vector) |
| \mathbf{A} | magnetic vector potential |
| A | z component of magnetic vector potential |
| \mathbf{B} | magnetic flux density |
| B_m | amplitude of maximum flux density |
| \mathbf{D} | electric flux density |
| \mathbf{E} | electric field strength |
| \mathbf{H} | magnetic field strength |
| h | burr width |
| \mathbf{J} | source current density |
| J | z-component of current density |
| \mathbf{P} | Jacobian matrix |
| p | loss per cubic meter |
| \mathbf{r} | residual vector |
| \mathbf{S} | stiffness matrix |
| \mathbf{T} | damping matrix |
| t | time variable |
| V | volume |
| W | energy |
| w | weighting function |
| w_{tot} | loss density |
| x | cartesian coordinates |
| y | cartesian coordinates |
| α | parameters defining boundary impedance condition |
| α | parameters experimentally obtained Steinmetz's equation |
| β | parameter defining boundary impedance condition |
| β | parameter defining type of time discretisation |
| γ | parameter defining boundary condition |
| Γ | boundary solution region |
| η | parameter of experimentally obtained Steinmetz's equation |
| ϕ | reduced scalar potential |
| μ_0 | permeability of air |
| μ | permeability of the material |
| ν | reluctivity of material |
| ρ | free charge density, resistivity of material |
| σ | conductivity of the material |
| ω | angular frequency |
| Ω | magnetic scalar potential |
| Ω | two dimensional solution region |

Subindices

| | |
|-----|-----------------------|
| air | air region |
| Fe | insulated iron region |
| ia | iron air interface |
| k | time steps |
| n | number of iterations |

Abbreviations

| | |
|-----|-------------------------------------|
| 1-D | one-dimensional |
| 2-D | two-dimensional |
| 3-D | three-dimensional |
| BEM | boundary element method |
| FEM | finite element method |
| ISO | international standard organisation |

1 Introduction

1.1 Background

The discovery of *magnesia* by sheperds in ancient part of Turkey led to the development of the first rotating device, Barlow's wheel (1821), the development in electric machines has never been stopped. The Barlow's wheel was developed a year after the discovery of electromagnetism by Faraday and the first three-phase cage induction motor was built by Dobrowolsky in 1889. Since then, machines have been easing human life and many inventions related to electric machines have been made. Research is still going on to optimise the efficiency of the machines.

Today, electrical machines are the driving horse of industry. The need of today's growing industry sector is energy efficient machines. The foremost thing in this venture is to identify the losses in the electrical machines. Losses in electrical machines can be broadly classified into electrical, mechanical and additional losses. Electrical losses occur as copper loss and iron loss. Copper losses are the ones that occur in windings of the machines. They depend on the number of phase, AC resistance of the phase winding and current. Iron loss on the other hand, comprises of hysteresis loss, eddy current loss and excess loss.

These losses add up the heat in electric machines and may damage the insulation and burn the machine in operating stage if the losses are not predicted accurately in design stage. The loss identification and its prediction using accurate numerical computation is essential for electric machine manufactures to design the proper cooling system and to save in maintenance cost. In loss identification process, the losses that can arise from manufacturing effect are not properly addressed. However, machine goes through a series of manufacturing process and in such process machine parameters and its material properties can be affected and can cause additional losses.

The time varying magnetic field in machines induces eddy currents in a ferromagnetic material which results in eddy current losses. Hence, the cores of electrical machines are built from thin laminated sheets. However, the inter-laminar sheets are not perfectly insulated, there might be foreign particles introduced during assembly and inspection. Moreover, the manufacturing process such as cutting and punching deteriorates and introduces the burrs at the edges of laminations. The burred lamination when stacked deteriorates the insulation of adjacent sheets and makes galvanic contacts which provides the conducting path for the eddy current through welding pass or bolts that are used to hold the stack. These circulating currents cause the additional losses and if these losses are not identified and treated properly, they may melt the insulation and damage the machine in operational stage.

1.2 Aim of thesis

The thesis is related to modelling the additional losses due to the manufacturing effect of electrical sheets. The primary aims of the thesis are as follows:

- To study about the iron loss and the effect of punching on the electrical sheets.
- To study and develop the numerical formulation to model the galvanic contacts at the edges of laminated sheets, couple it to 2-D finite element and validate it.
- To implement the developed coupled boundary layer formulation to 37 kW induction machine and compute the additional losses.

1.3 Outline of thesis

This thesis contains 5 chapters. Chapter 1 gives the overview of the problem and objectives of the thesis and in Chapter 2, iron loss and effect of punching is discussed and different numerical formulations for modelling the conducting layers are reviewed. In Chapter 3, methods of developing boundary layer formulation and its coupling to 2-D finite element is discussed. In Chapter 4, the implementation of the coupled boundary layer model for a 37 kW machine is done and finally the thesis work is concluded in Chapter 5.

2 Losses in sheets

2.1 Iron losses

Losses in ferromagnetic materials such as iron, nickel and their alloys can be calculated using Maxwell's equations and Poynting theorem. For a good conductor where the free charge density is zero, the following Maxwell's equations are viable [1] where \mathbf{E} , \mathbf{H} , \mathbf{B} , \mathbf{J} are electric field strength, magnetic field strength, magnetic flux density and current density, respectively.

$$\begin{aligned}\nabla \times \mathbf{E}(t) &= -\frac{\partial \mathbf{B}(t)}{\partial t} \\ \nabla \times \mathbf{H}(t) &= \mathbf{J}(t)\end{aligned}\quad (2.1)$$

Applying divergence theorem to a Poynting vector $[\mathbf{E}(t) \times \mathbf{H}(t)]$ and integrating over the enclosed volume V gives an expression representing the energy flow into the volume per unit time which is given by the

$$-\int_V \nabla \cdot [\mathbf{E}(t) \times \mathbf{H}(t)] dV = \int_V \left[\mathbf{H}(t) \cdot \frac{\partial \mathbf{B}(t)}{\partial t} + \mathbf{E}(t) \cdot \mathbf{J}(t) \right] dV. \quad (2.2)$$

Hence, for a stationary volume where the rate of flux density is $\frac{d\mathbf{B}(t)}{dt}$ and the the energy flow between interval of time t_1 and t_2 is given by,

$$W = \int_{t_1}^{t_2} \int_V \left[\mathbf{H}(t) \cdot \frac{d\mathbf{B}(t)}{dt} + \mathbf{E}(t) \cdot \mathbf{J}(t) \right] dV dt. \quad (2.3)$$

For an isotropic material where $\mathbf{B}(t)$ and $\mathbf{H}(t)$, $\mathbf{J}(t)$ and $\mathbf{E}(t)$ are in the same direction, equation (2.3) becomes equation (2.4). However in rotating magnetic field, the magnetic flux density lags the magnetic field strength due to hysteresis and the fields are not in same direction even in isotropic materials.

$$W = \int_V \left[\underbrace{\int_{B_1}^{B_2} H dB}_{\text{volumetric energy density}} + \underbrace{\int_{t_1}^{t_2} \frac{J^2(t)}{\sigma} dt}_{\text{Eddy loss}} \right] dV \quad (2.4)$$

Equation (2.4) obtained from solving Maxwell's equations gives the analytical expression for total iron loss where the first part, in left hand side of equation (2.4) is due to hysteresis loss that is graphically represented in Figure 1 and the second part of equation is associated with eddy current loss.

Hysteresis loss occurs due to movement and rotation of magnetic domains. Whenever the magnetic field is varied, reversible and irreversible movement of magnetic domains occur until it reaches to the saturation where all domains are turned in the

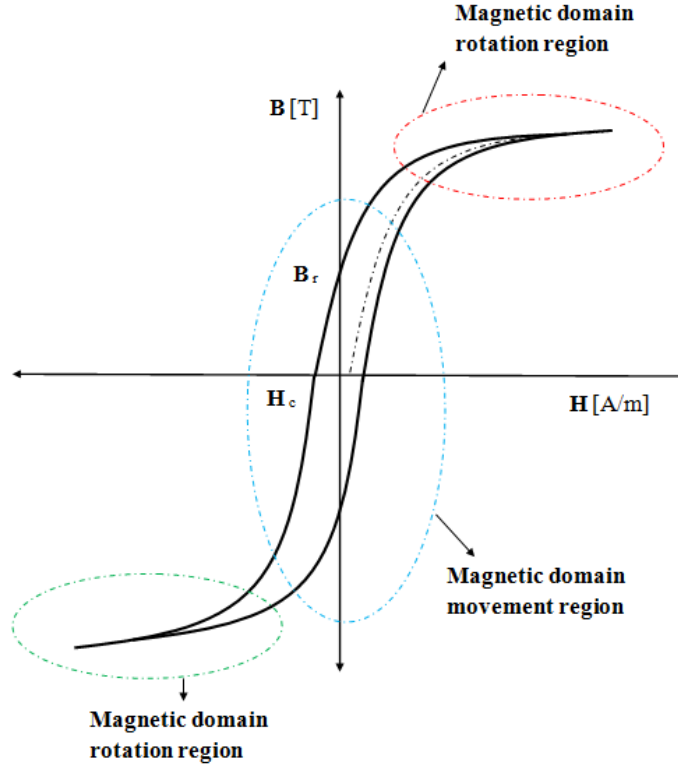


Figure 1: Hysteresis curve

same direction. This magnetic field variation causes the material to cycle through hysteresis curve where the part of supplied energy is lost. There are different models to determine the hysteresis loss such as Preisach model where macroscopic behavior of the material is assumed to results from an infinite number of rectangular loops [2] [3] [4] and Jiles-Atherton model where "sigmoid" shapes of hysteresis loops are considered [5]. However, the commonly used method to calculate the hysteresis loss for a sinusoidal induction is by using Steinmetz's equation which is given by

$$W_h = \eta B^\alpha . \quad (2.5)$$

The coefficients η and α are experimentally determined under a low frequency so that the eddy current will have minimum effect on the obtained coefficients. In case of non sinusoidal flux density, equation (2.5) is modified and the sum of harmonic components of flux density are considered. The eddy current loss is calculated as a function of electrical conductivity of material. The methods of its calculation will be discussed later. However, the experimentally obtained hysteresis loss and calculated eddy loss do not balance the measured total loss which gives rise to additional term called excess loss. The total iron losses of a magnetic sheet w_{tot} is given by equation (2.6) where B_m is the peak flux density, d is the sheet thickness, σ is the electrical conductivity, G is the friction coefficient, V_o is a parameter equivalent to coercitive field and S is the transversal area. [6]

$$\begin{aligned}
w_{\text{tot}} = \underbrace{\eta \mathbf{B}_m^\alpha \left[1 + \frac{0.65}{\mathbf{B}_m} \sum_{i=1}^n \Delta \mathbf{B}_i \right]}_{\text{Hysteresis loss}} + \underbrace{\frac{\sigma d^2}{12} \int_0^T \left(\frac{d\mathbf{B}(t)}{dt} \right)^2 dt}_{\text{Classical eddy current loss}} + \underbrace{\sqrt{\sigma G V_o S} \int_0^T \left| \frac{d\mathbf{B}(t)}{dt} \right|^{1.5} dt}_{\text{Excess loss}}
\end{aligned} \tag{2.6}$$

The excess loss was explained by Bertotti on the basis of a magnetic object [7]. According to the concept, the movement of the magnetic wall domain dislocate the other domain wall and they all correlate and form a magnetic object. The movement of newly formed magnetic object creates a current which needs to be compensated by external field and causes the excess loss.

The segregation of iron losses eases the loss identification and minimisation process. It is important to note that the input parameters for loss calculation are obtained experimentally from an Epstein frame and such assumption on input parameter are insufficient to model the loss accurately. In practical scenario, the electrical machine goes through different manufacturing processes such as rolling, punching and cutting of the sheets to the final assembly of machine parts. These processes deform the sheets and introduce a residual stress that has an impact on the magnetic properties of the sheet. The behavior of magnetic properties and iron loss under such stress is studied in [8], [9], [10], [11] where the increase in hysteresis loss was observed due to change in permeability. It was observed in [12] that an annealing process reduces iron losses by 50 % and produces a factor 3 change in permeability of test samples of laminated sheets.

The cores of the electrical machines and transformers are usually laminated and insulated to reduce the eddy current losses. Even with the insulated sheets, there can be additional losses due to the failure of insulation and the formation of burr. The additional eddy current losses are discussed in the following sections.

2.2 Interlaminar faults

The laminated sheets are not always perfectly insulated from each other. The laminated sheets are subjected to many foreign particles during assembly and in case of stator cores of machines, inter-laminar insulations are deteriorated due to mechanical damage during assembly of rotor and stator or arcing from winding failure [13]. The electromagnetic core imperfection detector tests [14, 15] are usually done to identify the inter-laminar faults of stator cores of the large machines. During the test, the stator cores are excited about 4 % of the operating flux and the fault current is detected by using a Chattock potentiometer. It is placed across the teeth of the core and measures the magnetic potential difference between the two ends. In a fault free case, it measures the magnetic potential difference which is in a phase with the exciting current. In a faulted case, it measures the magnetic field result from faulted current. Since, the fault circuit is resistive, the faulted current is in phase with the fault voltage and in phase quadrature with the excitation current.

Finally, the quadrature component of fault current is separated from the excitation current using a phase sensitive detector and hence, the fault current is identified.

The damaged sheets allow the eddy current to flow through the sheets and causes localised heating in the stator core and may cause the burning of the cores as shown in Figure 2. The identification of the fault through measurement is more or less accurate if the fault region is near the teeth of the core but if the fault is far from the teeth region, the fault identification through measurement is not sufficient and requires numerical formulation.



Figure 2: Inter-laminar insulation failure of stator core [13]

The focus of the thesis is to model the additional losses due to the formation of burrs on the edges of lamination during manufacturing process, and hence it is explained in the following section.

2.3 Burr formation

Steel sheets are an indispensable constituent in the construction of the cores of electromagnetic devices. Sheets are rolled to their given thickness and are laminated to minimise the eddy current loss. Later, they are cut or punched into desired shape for electromagnetic device. Sheets are laminated or coated before they are cut or punched to ease the punching and welding process. Coating is done before punching to prevent the damage to the cutting tools and the sheet itself [16].

The required shape is obtained by cutting techniques, such as punching, guillotine, laser cutting, photocorrosion and all these result in cut edges. The cutting techniques cause the variation in losses. It was observed in [8] that the measured loss variation was upto 10 % to 20 % for 60 Hz 1.5 T. They also claimed that among these cutting techniques laser cutting has the biggest effects on sheets. The sheets obtained from different cut are shown in Figure 3.

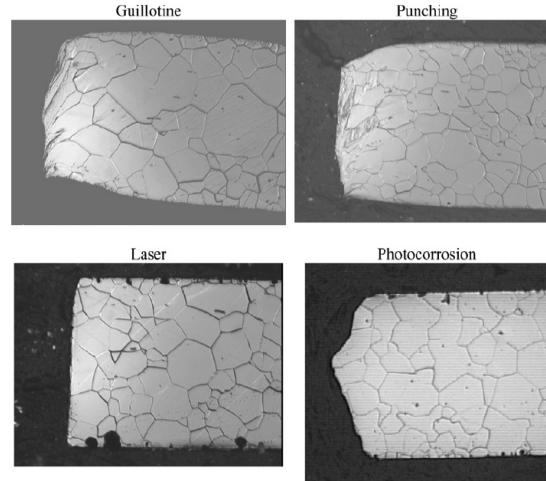


Figure 3: Sheets obtained from different cutting technique [17]

Punching and cutting induce internal mechanical stresses and deteriorate the magnetic properties of the sheet. This behaviour becomes very important in high Si-alloyed grades of non-oriented electrical steel [18]. According to Schmidt [19], when cutting by punching, stress region can be from 0.35 mm upto 10 mm [20] from the cut edge and the deformed area can extend for about 0.3 mm due to plastic deformation [17]. However, engineering society has also agreed upon the average affected cut edge, having a width equal or larger than the thickness of the lamination [21]. Cutting of the steel not only deteriorates the magnetic properties of the steel but also causes inter-laminar short circuits due to burr formation.

Burr and clearance have a strong impact on interlayer short-circuits as well as on the cut edge properties. Burr formation occurs due to shearing and it occurs during the separation of the metal by the two blades of the guillotine. Series of the events occur, in which the moving blade contacts the sheet and rolls over till it reaches the fracture shear stress of the sheet. The continuation of load continues initiates a crack which produces the rapid breakthrough involving a ductile fracture of sheet and formation of a burr as shown in Figure 4. In [22] Ko based on his work defines burr as "undesirable projection of material formed as the result of plastic flow from a cutting or shearing operation". The ISO 13715 defines the edge of a workpiece as burred if it has an overhang greater than zero [23]. In [24] Gillespie has however defined different types of burrs such as possion burr, rollover burr, tear burr and cut-off burr as shown in Figure 5.

These burrs certainly deteriorate the properties of the materials in deformed region and may cause the short-circuits between the laminated sheets by impairing the insulation of adjacent sheets in case of cores of electric machines. However, there are many de-burring techniques such as using electrochemical machining, abrasive flow machining or high pressure water jet. Unfortunately, no single de-burring op-

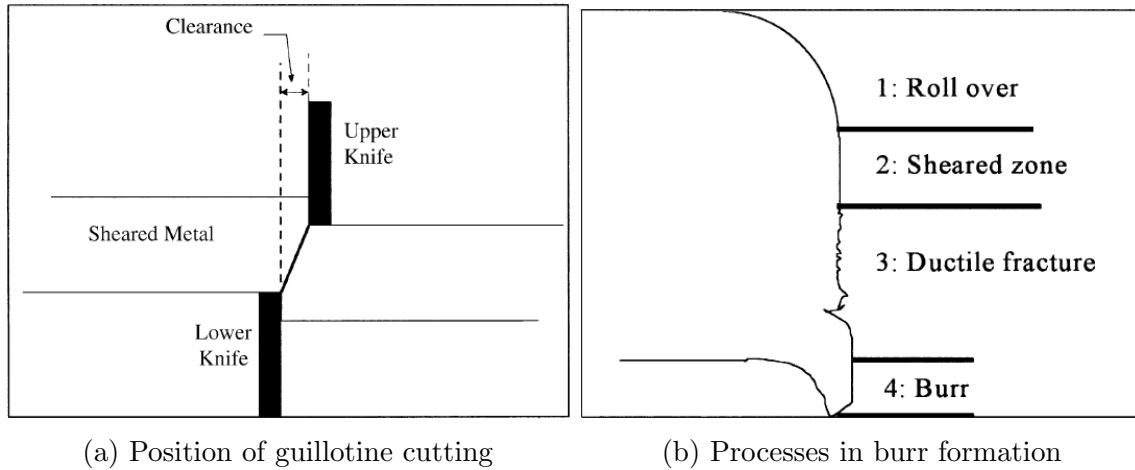


Figure 4: Burr formation [9]

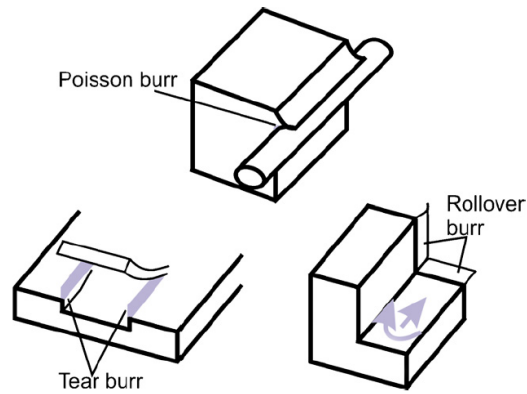


Figure 5: Types of burr [24]

eration can accomplish all required edge conditions without having side effects [25]. The burred edges impair the insulation of adjacent sheets during the stacking of the sheets and form the conducting layer. The effect of circulating eddy current will only occur if burrs occur on opposite edges of the laminations [26]. However, bolts or welding pass which are used to hold the stack of laminations can also provide the returning path for the eddy current to form the closed loop. The number of conducting layers formed by burrs within the stacks are uncertain since they are formed by the stochastic process and are random in nature as shown in Figure 6. These inter-laminar short circuits are accountable for additional losses in stack of sheets and are considered indeterminable. The losses generally depend on a large number of unknowns, such as e.g the short circuit's geometry, the conductivity of the contact points and the flux and eddy current distributions in its vicinity [27]. The total influence of all the short circuits can however be modelled by numerous formulations.

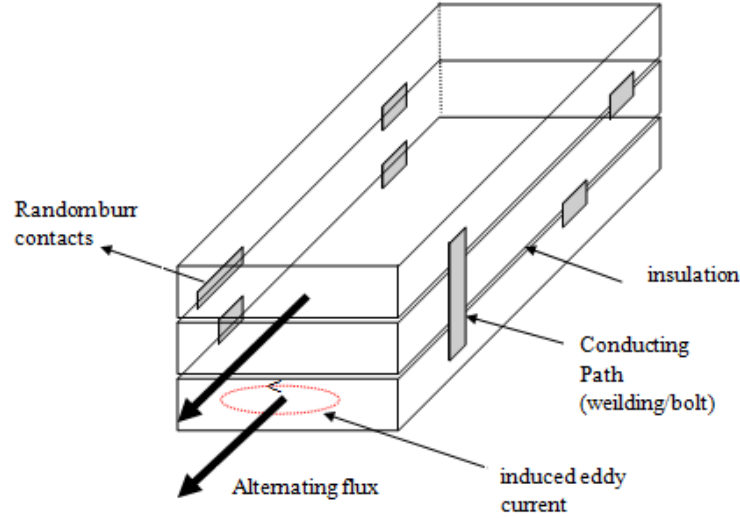


Figure 6: Schematic diagram of the induced eddy current and galvanic contacts on electrical sheets

2.4 Literature review: Modeling formulations

There have been few studies done in [28], [26] regarding the modeling of inter-laminar short circuit losses using artificial burr contacts where effect on permeability due to punching is assumed constant and randomness of burr contacts were not completely addressed. Eddy current loss was calculated due to galvanic contacts on three phase transformer assuming the artificial burr by clamping conducting copper tape at the opposite end of the limbs as shown in Figure 7. It was assumed that x component of eddy current loss circulated along the length of the burr and y component circulated only in a thickness of burr ($8 \mu\text{m}$). Eddy current loss was calculated analytically using equation (2.7) and measured experimentally by varying the number of laminations affected by the burrs. The comparison of calculated and measured loss revealed that the measured eddy loss decreased compared to the calculated one as the the contacts of laminations were increased. This is because the magnetic flux density was considered uniform in the burred region during analytical calculation but during experimental study exactly opposite burr contacts caused the eddy current to oppose the magnetizing field and reduce the flux density in burred region and hence decreased the experimental losses.

$$p = \underbrace{\frac{\pi^2 f^2 B_m^2 l^2}{6\rho}}_{\text{eddy current loss along } x \text{ direction}} + \underbrace{\frac{4\pi^2 f^2 B_m^2}{\rho} \left(\frac{1}{3} \left(\left(\frac{b}{2} + h \right)^3 - \frac{b^3}{8} \right) \right)}_{\text{eddy current loss along } y \text{ direction}} \text{ W/m}^3 \quad (2.7)$$

Similarly, Moses et al. [29] studied the effect of the burrs on the large transformers.

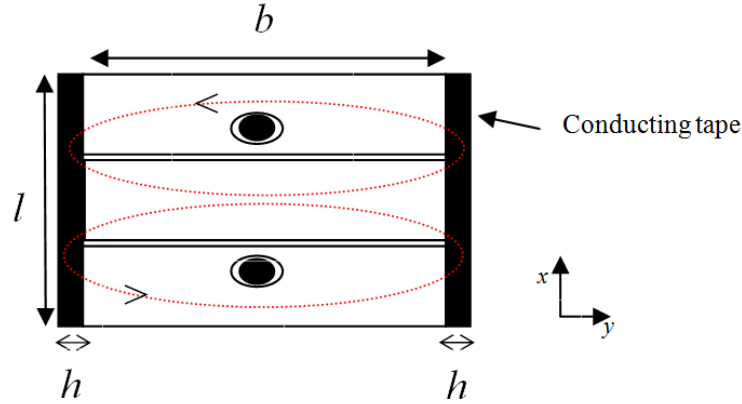
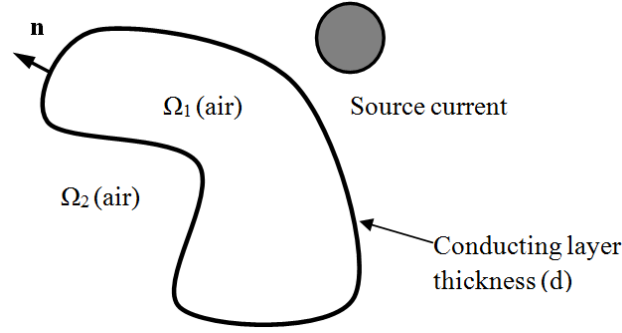


Figure 7: Cross section of lamination with artificial burrs

For a grain oriented 3 % silicon iron of 0.28 mm sheets burr size lesser than 0.02 mm was observed. Moses drilled the laminated sheets to have the controllable artificial contacts. The contacts were varied by inserting conducting pins. They used the microprocessor controlled thermistor bridge to scan the temperature and measured the loss on temperature rise principle. They concluded the increase of the loss due to burr contacts probably up to 5 % of the total loss.

The burred edges can be modeled with finite element method with a very fine mesh layer and usually an adaptive meshing is done but this fine mesh layer may consist of degenerated elements or very high number of elements. The degenerated elements lead to the system of ill conditioned matrix and may require costly solver and high computational time. The alternative of the fine mesh is to model the conducting layers formed by the burred edges by using boundary element method or thin shell elements. These methods have been used to model the conducting shield in rotors of high speed machines to damp mechanical oscillations and to prevent frequency noise [30].

If the curl of a vector field has to be zero for a regions, vector field and its derivative should be defined i.e. region should be simply connected domain and while modeling the thin conducting layer in 3-D, if a multiple connected domain is present, a cut should be introduced to make it simply connected domain so that the curl of a field can be zero and the Green's function can be applied. In 3-D conducting layers are modeled with magnetic scalar potential but requirement of the simple connected domain is a limitation. Hence, Honma et al. [31] modeled the thin conducting layer having conductivity σ , thickness d and permeability μ , using the magnetic vector potential to express a boundary impedance condition and a boundary element method to solve the boundary integral equation. The boundary impedance condition equation (2.8) for thin magnetic conducting layer Γ as shown in Figure 8 was obtained by solving the ampere's law under quasi-static approximation and expressed in magnetic vector potential as

Figure 8: Closed boundary Γ

$$\begin{bmatrix} A_1 \\ \frac{\partial A_1}{\partial n} \end{bmatrix} = \frac{1}{1 - \alpha\beta} \begin{bmatrix} 1 + \alpha\beta & 2\beta \\ 2\alpha & 1 + \alpha\beta \end{bmatrix} \begin{bmatrix} A_2 \\ \frac{\partial A_2}{\partial n} \end{bmatrix} \quad (2.8)$$

where,

$$\alpha = \frac{\sigma\omega\mu_0 \tanh(\frac{\gamma d}{2})}{j\gamma}, \quad \beta = \frac{j\gamma \tanh(\frac{\gamma d}{2})}{\sigma\omega\mu_0}$$

$$\gamma = \sqrt{(j\omega\sigma\mu)}.$$

The integral equation governing the quasistatic magnetic field of thin layer in the air regions Ω_1 and Ω_2 as shown in Figure 8 are derived from the Laplace equation for A where the thickness of layer was neglected in geometrical sense. The influence of thickness was compensated by imposing impedance boundary conditions. The integral equation was discretized by using boundary element method (BEM). BEM has an advantage of reducing the number of data since it reduces the dimension of mesh on physical model by one. In case of 2-D analysis, meshing is only done along the boundaries of the geometry and is suitable if the computation interest is only in the boundaries of domain. However, BEM is suited to deal with problems relating to infinite domains but not appropriate for non-linear problems. [32]

Similarly, Muller et al. [33] developed the static and harmonic case formulation for conducting shell based on boundary equations. The differential equations were derived on the principle that current in the shell causes the discontinuity of the tangential component of magnetic field strength. The derived equation of the shell was coupled with boundary integral equations describing 3-D domains and was discretised by surface finite element mesh with respectively a point collocation method for boundary integral equation and variational method for shell. For a 3-D domain Muller addressed both the cases of closed and open shell. In case of closed shell, two independent boundary integral equations were developed and in case of open shell only one equation was developed.

There have also been studies done where the conducting layers are modeled with thin shell elements. [34] Dular et al. developed the dual formulations to study the thin conducting layers for 3-D problems and in [35, 36] 1-D thin shell model was

developed incorporating non-linearity using the formulations developed in [34]. The two formulations, vector potential formulation and magnetic field formulation were developed for 3-D problems. The thin shell boundary having thickness d was considered and the thin shell domain Ω_s which is not the part of domain Ω , was reduced to an average surface Γ_s situated halfway between inner surface and outer surface as shown in Figure 9.

The tangential discontinuity of electric field across the shell was addressed by decomposing vector potential \mathbf{a} into continuous \mathbf{a}_c and discontinuous \mathbf{a}_d term. The vector potential \mathbf{a} is uniquely defined in conducting region and decomposed part addressed the shell region. The thin shell was reduced assuming the discontinuous \mathbf{a}_d equal to zero on the inner side of the shell Γ_s^- and neglecting the corner and extremities effect in the shell. Hence, the governing equation is given by

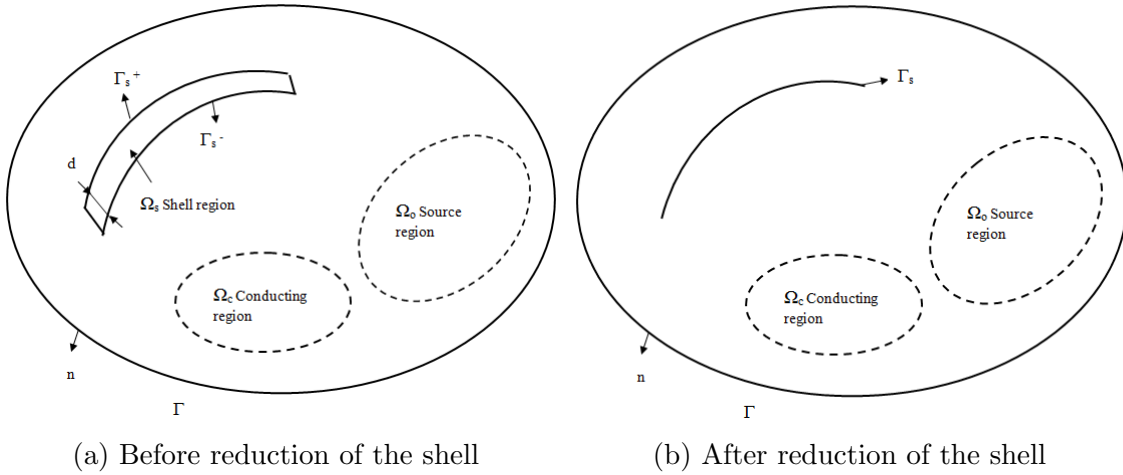


Figure 9: Thin shell formulation

$$\begin{aligned}
& \int_{\Omega} \nu (\nabla \times \mathbf{a}) \cdot (\nabla \times w) d\Omega + \int_{\Omega_c} \sigma \frac{\partial \mathbf{a}}{\partial t} \cdot w d\Omega + \int_{d\Omega/\Gamma_s} (\mathbf{n} \times \mathbf{H}) \cdot w d\Omega \\
& + 2 \int_{\Gamma_s} \sigma \beta \frac{\partial \mathbf{a}_{c,t}}{\partial t} \cdot w_c d\Gamma_s + \int_{\Gamma_s} \sigma \beta \frac{\partial \mathbf{a}_{d,t}}{\partial t} \cdot w_c d\Gamma_s + \int_{\Gamma_s} \sigma \beta \frac{\partial \mathbf{a}_{c,t}}{\partial t} \cdot w_d d\Gamma_s \quad (2.9) \\
& + \frac{1}{2} \int_{\Gamma_s} \sigma \beta \frac{\partial \mathbf{a}_{d,t}}{\partial t} \cdot w_d d\Gamma_s + \frac{1}{2} \int_{\Gamma_s} \frac{\mathbf{a}_{d,t}}{\mu \beta} \cdot w_d d\Gamma_s = \int_{\Omega_o} \mathbf{J}_o \cdot w d\Omega.
\end{aligned}$$

Equation (2.9) was discretized by whitney edge elements where w is the test function and $\beta = d/2$ if skin depth is larger than thickness of the shell. The advantage of the edge element is that its degree of freedom depends on the edge of the element and it can be interpreted as circulation of the field along the edge and moreover the tangential component of the vector potential ($\mathbf{a}_{c,t}, \mathbf{a}_{d,t}$) or surface gradient of magnetic scalar potential can be directly obtained from edge elements.

The above explained models are mostly focused on 3-D problems and hence the two dimensional boundary layer model was developed to address the conducting layers formed by the burrs in laminated sheets. The width of the layer was considered to be less than skin depth and was coupled to the existing 2-D finite element equations in inhouse software FCSMEK. The formulation of the boundary layer model is more discussed in the later section.

3 Methodology

3.1 Finite element method

A finite element method is a numerical computational tool for solving the partial differential equations in the field of science and engineering. The history of finite element dates back to the work of Lord Rayleigh (1870) and W. Ritz (1909) on variational methods and weighted residual approach of B.G. Galerkin (1915) which formed the theoretical background for finite element [37]. The "finite element" term was coined by Ray W. Clough in 1976, and since then finite element method has been exploited by so many researchers from the field of mathematics, engineering and applied science.

The use of variational or residual method for solving the partial differential equation requires choosing of a quality approximation function for the entire geometry of interest. The chosen approximation function also needs to satisfy essential boundary conditions which becomes tedious as the geometry becomes complex. So, with the use of finite element method, complex geometry can be divided into simple domains or elements where suitable algebraic polynomials can be used as approximation function over the elements. Later, those elements can be assembled based on the continuity of the solution to represent the entire geometry.

In electromagnetism, FEM is performed with the residual method since the residual method is established directly from the physical equation that has to be solved and is more simpler to apply compared to the variational method [6]. In [38] Luomi also explained the application of the finite element method with the numerical solution of the magnetic field and the eddy current problems in electric machines. The fundamentals of the finite element method and governing equation of the electromagnetic field solution for electrical machines are discussed in the following.

The quasi-static case ($\frac{\partial \mathbf{D}}{\partial t} = 0$) of Maxwell's equation can be expressed as following

$$\nabla \times \mathbf{E} = -\frac{\partial \mathbf{B}}{\partial t} \quad (3.1)$$

$$\nabla \times \mathbf{H} = \mathbf{J} \quad (3.2)$$

$$\nabla \cdot \mathbf{B} = 0 \quad (3.3)$$

The material equation is given by

$$\mathbf{B} = \mu \mathbf{H} \quad (3.4)$$

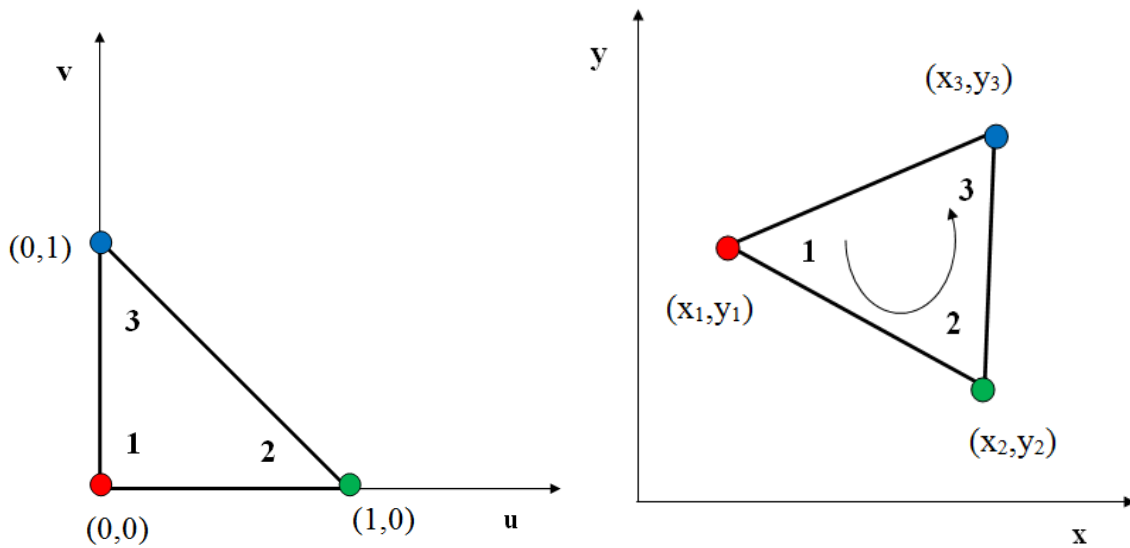
$$\mathbf{J} = \sigma \mathbf{E} \quad (3.5)$$

The electromagnetic field solution is obtained by simplifying the Maxwell's equation

and solving the partial differential equation. The application of the finite element with residual method in solving the above equations requires the space discretisation of the domain where these equations are solved. The time-dependent term in the equation requires time discretisation. Moreover, the non-linearity introduced by the material properties is governed by equation (3.4) and should be taken into account during computation. The space, time discretisation and non-linearity are discussed briefly in the following section.

3.1.1 Space discretization

The solution region is discretized in space by dividing the problem region into finite elements and a shape function is defined over each single element. The space discretisation is also called as meshing and the accuracy of the solution depends upon the order of the interpolating polynomials or the shape functions. The type of element in meshing depends upon the geometry. For 2-D space, meshing is done with triangular or quadrilateral elements and for 3-D tetrahedral or hexahedral elements are generally used. The order of the interpolating functions is chosen by trading off between the computation cost and the accuracy. In this thesis a boundary layer formulation is coupled with a 2-D finite element formulation in an inhouse software. First order triangular elements were used as shown in Figure 10.



(a) First order triangular element in local $u-v$ plane (b) First order triangular element in global $x-y$ plane

Figure 10: Triangular element and its coordinate transformation

Each shape function of triangular element is non-zero over to only those elements that contain its nodal points and equals zero over all other elements. The first node of a triangular element is selected freely and nodes are numbered anticlock-

wise. Shape functions for each element are firstly defined in the local or reference element as in Figure 10a. Later, locally defined shape functions are transformed into the global $x - y$ coordinates plane as in Figure 10b by multiplying with coordinate transformation Jacobian matrix.

3.1.2 Time discretization

The time derivative term in equation (3.1) can be discretized by θ -algorithm [6] which allows the variable to be expressed for time (t) and increment of time ($t + \Delta t$). The boundary layer formulation derived in section 3.3 is based on the magnetic vector potential where the magnetic flux density \mathbf{B} in equation (3.1) is written as curl of the magnetic vector potential. The time derivative term of the magnetic vector potential is then solved by using a time step by step procedure where the time steps are denoted by k and $k+1$.

$$\mathbf{a}^{k+1} = \mathbf{a}^k + \left[\beta \frac{\partial \mathbf{a}}{\partial t} |^{k+1} + (1 - \beta) \frac{\partial \mathbf{a}}{\partial t} |^k \right] \Delta t \quad (3.6)$$

The term β in equation (3.6) determines the type of discretization. There are usually three methods, the first one is forward Euler ($\beta = 0$) which is simple but bit unstable, the second one is backward Euler ($\beta = 1$) which is stable for non-linear equation since it gives explicit equations in output variables and the third one is Crank-Nicolson ($\beta = 0.5$) method. The backward Euler method damps the error and consumes energy but Crank-Nicolson method does not damps the error and conserves energy. Time discretization allows to obtain the field solution at each time step through the iterative process and from those field solutions transient study of machine is done.

3.1.3 Non-linearity

The non-linearity is introduced by the material characteristics. In such case, $\nu = 1/\mu$ depends on the square of magnetic flux density which results in non-linear equations and these non-linear equations should be solved iteratively by linearising the equations. The linearisation is done by Newton Raphson method where nodal value of each element is corrected at each time step of k by n number of iterations by

$$\mathbf{a}_n^k = \mathbf{a}_{n-1}^k - \mathbf{P}^{-1} \mathbf{r}(\mathbf{a}_{n-1}^k) \quad (3.7)$$

where, \mathbf{r} is the residual vector and \mathbf{P} is the Jacobian matrix given by,

$$\begin{aligned} \mathbf{r}(\mathbf{a}^k) &= 0 \\ \mathbf{P} &= \frac{\partial \mathbf{r}(\mathbf{a}^k)}{\partial \mathbf{a}^k}. \end{aligned}$$

3.2 Eddy current formulation

The time varying magnetic field induces the eddy current. The direction of induced current is given by the right hand thumb rule and it can be mathematically represented in equation (3.1) and equation (3.2). In [38] Luomi presented two basic formulations for the eddy current problems using the magnetic vector potential (\mathbf{A}) and the electric vector potential (\mathbf{T}).

The curl of magnetic vector potential gives the magnetic flux density and is given by

$$\mathbf{B} = \nabla \times \mathbf{A}. \quad (3.8)$$

Equation (3.8) can be substituted in equation (3.2) and current density (\mathbf{J}) is expressed in terms of magnetic vector potential

$$\nabla \times (\nu \nabla \times \mathbf{A}) = \mathbf{J}. \quad (3.9)$$

It should be noted that equation (3.9) is valid for all magneto-static problems and it is also valid for eddy current problems. The only difference is in case of eddy current problem \mathbf{J} is the induced current density that is given by equation (3.10) and obtained by solving equations (3.8),(3.9), (3.1) and (3.5).

$$\nabla \times (\nu \nabla \times \mathbf{A}) = -\sigma \frac{\partial \mathbf{A}}{\partial t} - \sigma \nabla \phi. \quad (3.10)$$

where, ϕ is the reduced scalar potential and $\nabla \phi$ is the irrotational part due to electric charges and the polarization of dielectric materials. Hence, the expression for the magnetic vector potential formulation for eddy current problem is given by

$$\nabla \times (\nu \nabla \times \mathbf{A}) + \sigma \frac{\partial \mathbf{A}}{\partial t} + \sigma \nabla \phi = \mathbf{J}_s. \quad (3.11)$$

Equation (3.11) assumes that for a current carrying region there is either a source current density or eddy current density. In the presence of current source density, conductivity (σ) is zero and equation (3.11) becomes equation (3.9). In presence of eddy current density, the source current density $\mathbf{J}_s = 0$ and equation (3.11) becomes equation (3.10). As, the eddy current closes itself, the divergence of the eddy current density vanishes and gives another equation as

$$\nabla \cdot \left(\sigma \frac{\partial \mathbf{A}}{\partial t} + \sigma \nabla \phi \right) = 0. \quad (3.12)$$

The continuity conditions of the field at the interface is also satisfied since the tangential component of electric field ($\frac{\partial \mathbf{A}}{\partial t} + \nabla \phi$) and the normal component of ($\sigma \frac{\partial \mathbf{A}}{\partial t} + \sigma \nabla \phi$) is continuous at boundary interface but this formulation does not ensure the continuity of tangential magnetic field.

Another eddy current formulation is the $\mathbf{T}-\Omega$ formulation where the magnetic field is defined in terms of electric vector potential \mathbf{T} and magnetic scalar potential Ω ,

$$\mathbf{H} = \mathbf{T} - \nabla\Omega. \quad (3.13)$$

The uniqueness of electric vector potential is obtained by Coulomb gauge as

$$\nabla \cdot \mathbf{T} = 0. \quad (3.14)$$

Equation (3.13) combined with equation (3.2) gives

$$\nabla \times \mathbf{T} = \mathbf{J}. \quad (3.15)$$

The electric field can be expressed in terms of obtained current density as

$$\mathbf{E} = \frac{1}{\sigma} \nabla \times \mathbf{T}. \quad (3.16)$$

Solving the Maxwell's equations (3.1),(3.4),(3.13) and (3.16), the electric vector formulation is obtained as

$$\nabla \times \left(\frac{1}{\sigma} \nabla \times \mathbf{T} \right) = - \frac{\partial [\mu(\mathbf{T} - \nabla\Omega)]}{\partial t}. \quad (3.17)$$

The divergence of magnetic flux density vanishes $\nabla \cdot \mathbf{B} = 0$ and from this another equation is obtained as

$$\nabla \cdot \mu(\mathbf{T} - \nabla\Omega) = 0. \quad (3.18)$$

This formulation ensures the continuity of tangential component of magnetic field so the tangential component of vector potential \mathbf{T} is continuous at the interface also normal component of $\mu(\mathbf{T} - \nabla\Omega)$ is continuous at the interface.

3.3 Boundary layer formulation

The mathematical equation for the coupled boundary layer model for inter-laminar short circuit is derived on the basis that the presence of surface current at the edges of sheets causes a discontinuity of magnetic field. In magnetic field problems non-linear permeability of the material depends on the magnetic field strength and flux density. Thus, across a surface, the tangential component of the magnetic field and the normal component of the magnetic flux density are continuous. However, a linear current density or free surface current on edges causes the discontinuity of the tangential component of the magnetic field strength. The relation is shown in equation (3.19) and to derive the expression it is assumed that thin slab is perpendicular to a x axis and \mathbf{J} is constant in the thin conducting layer h and is perpendicular to the plane as shown in Figure 11.

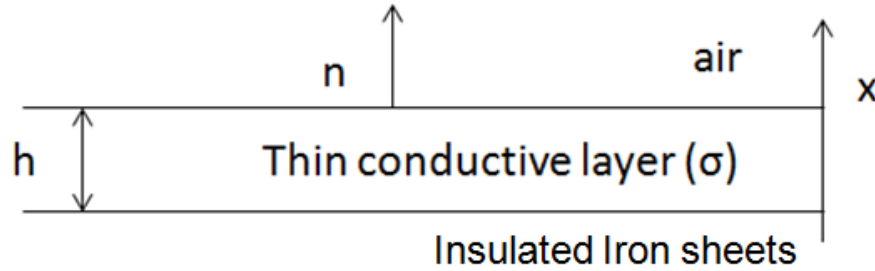


Figure 11: Thin slab

$$\mathbf{n} \times (\mathbf{H}_1 - \mathbf{H}_2) = \int_0^h \mathbf{J} dx \quad (3.19)$$

The current density \mathbf{J} in terms of the magnetic vector potential is given in equation (3.9) and equation (3.10). Integrating the \mathbf{J} along the conducting layer and assuming there is no imposed potential difference, equation (3.19) becomes

$$\mathbf{n} \times (\mathbf{H}_1 - \mathbf{H}_2) = -\sigma h \frac{\partial \mathbf{A}}{\partial t}. \quad (3.20)$$

The magnetic field can be expressed in terms of magnetic flux density using the material equation (3.4) where ν_1 and ν_2 represents the reluctivities of insulated sheet and air, respectively.

$$\begin{aligned} \mathbf{n} \times (\nu_1 \mathbf{B} - \nu_2 \mathbf{B}) &= -\sigma h \frac{\partial \mathbf{A}}{\partial t} \\ \mathbf{n} \times (\nu_1 \nabla \times \mathbf{A} - \nu_2 \nabla \times \mathbf{A}) &= -\sigma h \frac{\partial \mathbf{A}}{\partial t} \end{aligned} \quad (3.21)$$

The magnetic vector potential (\mathbf{A}) in a two dimensional case is in z direction (A) and the curl of the magnetic vector potential becomes

$$\mathbf{n} \times \left(\nu_1 \frac{\partial A}{\partial y} \mathbf{i} - \nu_1 \frac{\partial A}{\partial x} \mathbf{j} \right) - \mathbf{n} \times \left(\nu_2 \frac{\partial A}{\partial y} \mathbf{i} - \nu_2 \frac{\partial A}{\partial x} \mathbf{j} \right) = -\sigma h \frac{\partial A}{\partial t} \mathbf{k}. \quad (3.22)$$

The normal (\mathbf{n}) is decomposed in x and y component in the two dimensional plane and the cross product of vectors is taken. Equation (3.22) becomes

$$\begin{aligned} \begin{bmatrix} \mathbf{i} & \mathbf{j} & \mathbf{k} \\ n_x & n_y & 0 \\ \nu_1 \frac{\partial A}{\partial y} & -\nu_1 \frac{\partial A}{\partial x} & 0 \end{bmatrix} - \begin{bmatrix} \mathbf{i} & \mathbf{j} & \mathbf{k} \\ n_x & n_y & 0 \\ \nu_2 \frac{\partial A}{\partial y} & -\nu_2 \frac{\partial A}{\partial x} & 0 \end{bmatrix} &= -\sigma h \frac{\partial A}{\partial t} \mathbf{k}, \\ \begin{bmatrix} -n_x \nu_1 \frac{\partial A}{\partial x} & -n_y \nu_1 \frac{\partial A}{\partial y} \end{bmatrix} \mathbf{k} - \begin{bmatrix} -n_x \nu_2 \frac{\partial A}{\partial x} & -n_y \nu_2 \frac{\partial A}{\partial y} \end{bmatrix} \mathbf{k} &= -\sigma h \frac{\partial A}{\partial t} \mathbf{k}. \end{aligned} \quad (3.23)$$

The gradient of A is a vector quantity expressed in equation (3.34) and the normal can be expressed as ($\mathbf{n} = n_x \mathbf{i} + n_y \mathbf{j}$) vector. The dot product of two terms is expressed in equation (3.23) and it becomes

$$[-\nu_1 \nabla A \cdot \mathbf{n} + \nu_2 \nabla A \cdot \mathbf{n}] \mathbf{k} = -\sigma h \frac{\partial A}{\partial t} \mathbf{k}. \quad (3.24)$$

The surface current equation in terms of vector potential is given by,

$$\nu_1 \nabla A \cdot \mathbf{n} - \nu_2 \nabla A \cdot \mathbf{n} = \sigma h \frac{\partial A}{\partial t}. \quad (3.25)$$

Now, solving the Maxwell's equations,

$$\nabla \times \nabla \times \mathbf{A} = \nabla(\nabla \cdot \mathbf{A}) - \nabla^2 \mathbf{A} = \mu \mathbf{J}, \quad (3.26)$$

and applying Coloumb gauge, $\nabla \cdot \mathbf{A} = 0$ in the equation (3.26), the partial differentiation equation (3.26) becomes

$$-\mathbf{k} \left[\frac{\partial}{\partial x} \left(\nu \frac{\partial A}{\partial x} \right) + \frac{\partial}{\partial y} \left(\nu \frac{\partial A}{\partial y} \right) \right] = J \mathbf{k}. \quad (3.27)$$

The partial differential equation in two dimensional can be written as

$$\nabla \cdot (\nu \nabla A) = -J. \quad (3.28)$$

The non-conducting region R comprising insulated iron (Ω_{Fe}) and air (Ω_{air}) with surface current at the boundary as shown in Figure 12 is considered. The J in equation (3.28) will be zero because of the non-conducting regions. Now, according to the weighted residual method, multiplying equation (3.28) by the weight function w and integrating over the respective region, the following equations is obtained

$$R = \int_{\Omega} w \nabla \cdot (\nu \nabla A) d\Omega = \int_{\Omega_{\text{Fe}}} w \nabla \cdot (\nu_1 \nabla A) d\Omega + \int_{\Omega_{\text{ir}}} w \nabla \cdot (\nu_2 \nabla A) d\Omega = 0. \quad (3.29)$$

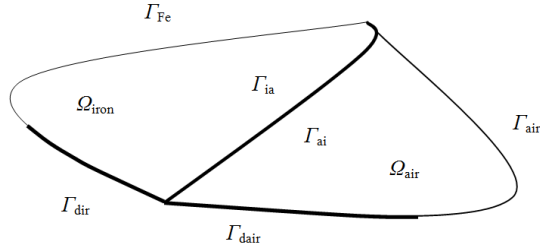


Figure 12: Definition of two region

Solving in insulated iron region

$$R_{\text{Fe}} = \int_{\Omega_{\text{Fe}}} w \nabla \cdot (\nu_1 \nabla A) d\Omega = - \int_{\Omega_{\text{Fe}}} \nu_1 \nabla A \cdot \nabla w d\Omega + \int_{\Omega_{\text{Fe}}} \nabla \cdot (\nu_1 \nabla A) w d\Omega = 0,$$

now, applying divergence theorem and Green's theorem to the second part of the equation gives

$$\int_{\Omega_{\text{Fe}}} \nabla \cdot (\nu_1 \nabla A) w d\Omega = \oint_{\Gamma} w (\nu_1 \nabla A) \cdot \mathbf{n} d\Gamma,$$

and assuming the weight function vanishes along the Dirichlet boundaries Γ_{dir} , the equation in insulated iron region becomes,

$$\int_{\Omega_{\text{Fe}}} \nu_1 \nabla A \cdot \nabla w d\Omega - \oint_{\Gamma_{\text{ia}}} w (\nu_1 \nabla A) \cdot \mathbf{n} d\Gamma - \oint_{\Gamma_{\text{Fe}}} w (\nu_1 \nabla A) \cdot \mathbf{n} d\Gamma = 0. \quad (3.30)$$

Solving in air region

$$R_{\text{air}} = \int_{\Omega_{\text{air}}} w \nabla \cdot (\nu_2 \nabla A) d\Omega = - \int_{\Omega_{\text{air}}} \nu_2 \nabla A \cdot \nabla w d\Omega + \int_{\Omega_{\text{air}}} \nabla \cdot (\nu_2 \nabla A) w d\Omega = 0,$$

applying the divergence theorem and Green's theorem to the second part of the equation gives

$$\int_{\Omega_{\text{air}}} \nabla \cdot (\nu_2 \nabla A) w d\Omega = \oint_{\Gamma} w (\nu_2 \nabla A) \cdot \mathbf{n} d\Gamma,$$

and assuming the weight function vanishes along the Dirichlet boundaries Γ_{dair} , the equation in air region becomes

$$\int_{\Omega_{\text{air}}} \nu_2 \nabla A \cdot \nabla w d\Omega - \oint_{\Gamma_{\text{ai}}} w (\nu_2 \nabla A) \cdot \mathbf{n} d\Gamma - \oint_{\Gamma_{\text{air}}} w (\nu_2 \nabla A) \cdot \mathbf{n} d\Gamma = 0. \quad (3.31)$$

Putting equation (3.30) and (3.31) in equation (3.29) gives,

$$R = \int_{\Omega_{\text{Fe}}} \nu_1 \nabla A \cdot \nabla w d\Omega + \int_{\Omega_{\text{air}}} \nu_2 \nabla A \cdot \nabla w d\Omega - \left(\oint_{\Gamma_{ia}} w(\nu_1 \nabla A) \cdot \mathbf{n} d\Gamma - \oint_{\Gamma_{ia}} w(\nu_2 \nabla A) \cdot \mathbf{n} d\Gamma \right) = 0 \quad (3.32)$$

where,

$$- \oint_{\Gamma_{ai}} w(\nu_2 \nabla A) \cdot \mathbf{n} d\Gamma = \oint_{\Gamma_{ia}} w(\nu_2 \nabla A) \cdot \mathbf{n} d\Gamma$$

The last term of equations (3.30) (3.31) defines homogeneous Neumann boundary condition $(\nu \nabla A) \cdot \mathbf{n} = 0$ and is satisfied naturally. The integrals over boundaries Γ_{ia} and Γ_{ai} have opposite normal vectors directed outwards from the region. The presence of surface current on the boundary causes the discontinuity of the tangential component of the magnetic field strength, the difference between these two integrals gives the surface current. The mathematical expression showing $(\nu \nabla A) \cdot \mathbf{n}$ as the tangential components of the magnetic field strength (H_t) is shown in equation (3.36) and its geometrical representation is shown in Figure 13.

The vector potential \mathbf{A} in two dimension is in z direction and the magnetic flux density is given by,

$$\mathbf{B} = [\mathbf{i} \quad \mathbf{j}] \begin{bmatrix} \frac{\partial A}{\partial y} \\ -\frac{\partial A}{\partial x} \end{bmatrix}. \quad (3.33)$$

The gradient of A can be expressed as

$$\nabla A = [\mathbf{i} \quad \mathbf{j}] \begin{bmatrix} \frac{\partial A}{\partial x} \\ \frac{\partial A}{\partial y} \end{bmatrix}. \quad (3.34)$$

Hence, magnetic flux density \mathbf{B} can be expressed in terms of ∇A with the introduction of matrix term as

$$\mathbf{B} = \begin{bmatrix} 0 & 1 \\ -1 & 0 \end{bmatrix} \nabla A. \quad (3.35)$$

Using equation (3.4) and taking the inverse of the matrix, $\nu \nabla A$ is expressed in terms of \mathbf{H} as

$$\nu \nabla A = \begin{bmatrix} 0 & -1 \\ 1 & 0 \end{bmatrix} \mathbf{H}. \quad (3.36)$$

Therefore, $\nu \nabla A \cdot \mathbf{n}$ is the tangential component of \mathbf{H} whose discontinuity leads to the surface current.

Multiplying the equation (3.25) by weight function w and taking the line integral along iron air interface ia , the following expression is obtained

$$\oint_{\Gamma_{ia}} w(\nu_1 \nabla A) \cdot \mathbf{n} d\Gamma - \oint_{\Gamma_{ia}} w(\nu_2 \nabla A) \cdot \mathbf{n} d\Gamma = \oint_{\Gamma_{ia}} w \sigma h \frac{\partial A}{\partial t} d\Gamma_{ia}. \quad (3.37)$$

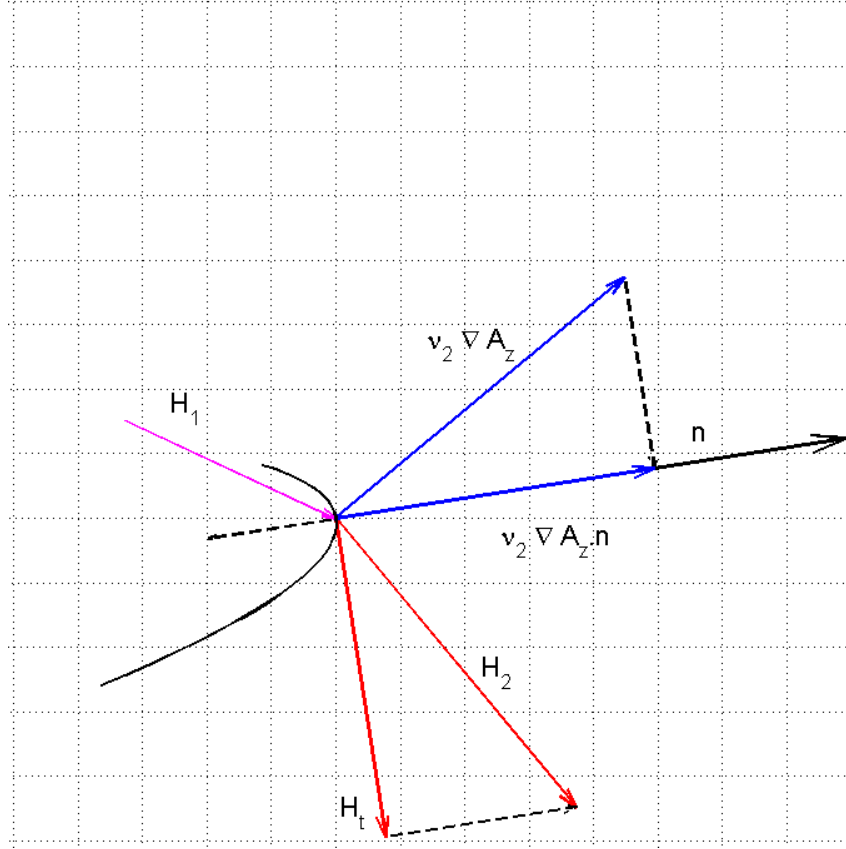


Figure 13: Geometrical representation as $\nu \nabla A \cdot \mathbf{n}$ as tangential component of \mathbf{H}

Putting the equation (3.37) in equation (3.32), the equation to be solved in insulated iron and air region is obtained as follows,

$$R = \int_{\Omega_{\text{Fe}}} \nu_1 \nabla A \cdot \nabla w d\Omega + \int_{\Omega_{\text{air}}} \nu_2 \nabla A \cdot \nabla w d\Omega - \oint_{\Gamma_{\text{ia}}} w \sigma h \frac{\partial A}{\partial t} d\Gamma_{\text{ia}} = 0. \quad (3.38)$$

3.4 Model Analysis

The derived mathematical boundary layer model given by equation (3.38) was compared in COMSOL MultiphysicsTM with a fine layer model. The fine layer model consisted of very fine mesh that has 950028 quadratic triangular elements. The model was compared on UI-electrical sheets as shown in Figure 14. The material of the UI sheet was iron having a relative permeability of 4000. The UI sheets were considered insulated and conductivity was assumed to be zero. However, along the edges of the sheets a conductivity of 3 MS/m was used.

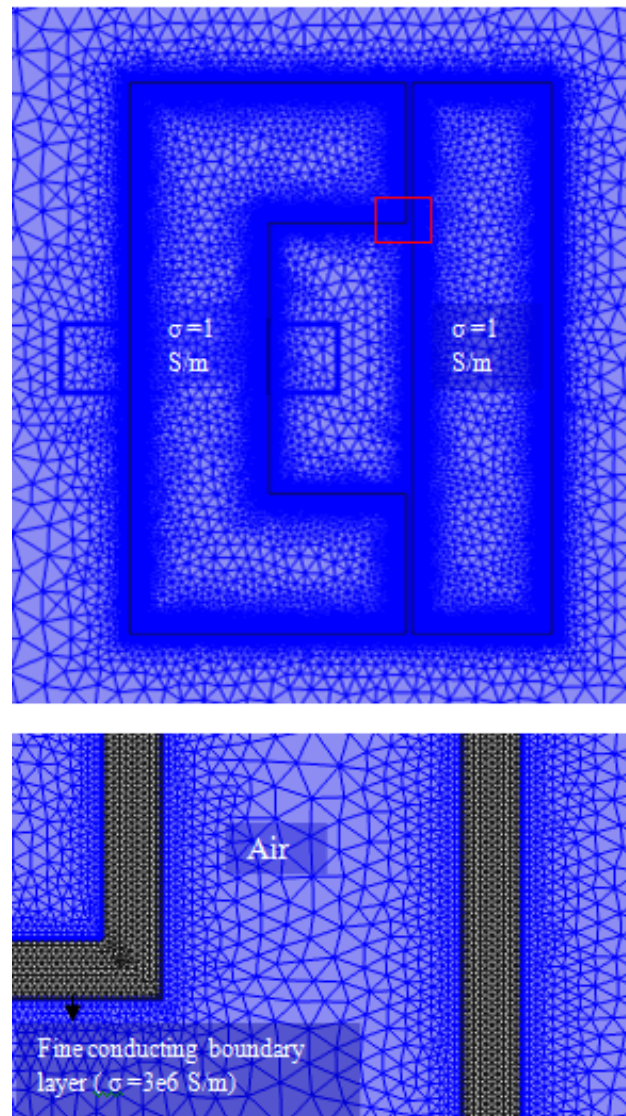
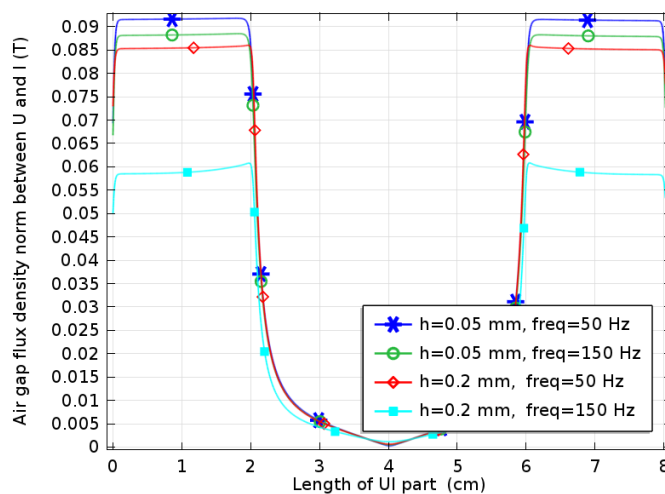
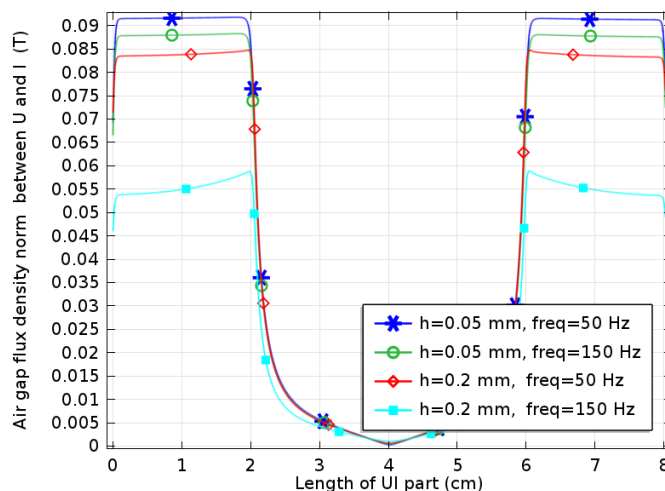


Figure 14: UI geometry

Both the models were studied in frequency domain, varying the frequency from 50 Hz to 150 Hz. In the fine mesh model of UI sheets, a thin conducting layer of width h was assumed and it was parametrized from 0.05 mm to 0.2 mm as shown in Figure 14. The loss was computed at each thickness and frequency. The boundary layer model was implemented by considering the same geometry and mesh. The thickness in the boundary layer model was varied in the formulation. The air gap flux densities between U and I sheets at different conducting layers and frequencies were plotted in Figure 15. It can be seen that there is not noticeable difference in the air gap flux densities between two models. The results are almost equal at low frequency and low conducting width. The induced losses in the conducting layer were also calculated in



(a) Air gap flux density between U and I sheet along the length in fine layer model



(b) Air gap flux density between U and I sheet along the length in boundary layer model

Figure 15: Comparison of air gap flux density

both the fine mesh model and boundary layer model supplying the external current

density of 1.5 A/mm^2 . The results are shown in Figure 16. The calculated losses from both the models were similar at 50 Hz and at burr width less than 0.1 mm. It is seen from Figure 16 that as the frequency increases the losses increase but at the frequency of 150 Hz after 0.15 mm, shielding phenomenon is seen which opposes the flux to penetrate through conducting layer and hence decreases the loss. However, the two models behave approximately in similar way. This model can later be used to model random contacts of sheets by varying the conductivity and burr width.

The random distribution of the conductivity and the width of conducting layer can be obtained by stochastic approach through measurement. The model was firstly incorporated in an inhouse software FCSMEK and non-linear model of UI90 sheets was studied in both FCSMEK and COMSOL MultiphysicsTM. The results were compared and later the model was applied to study the losses in a 37 kW induction machine.

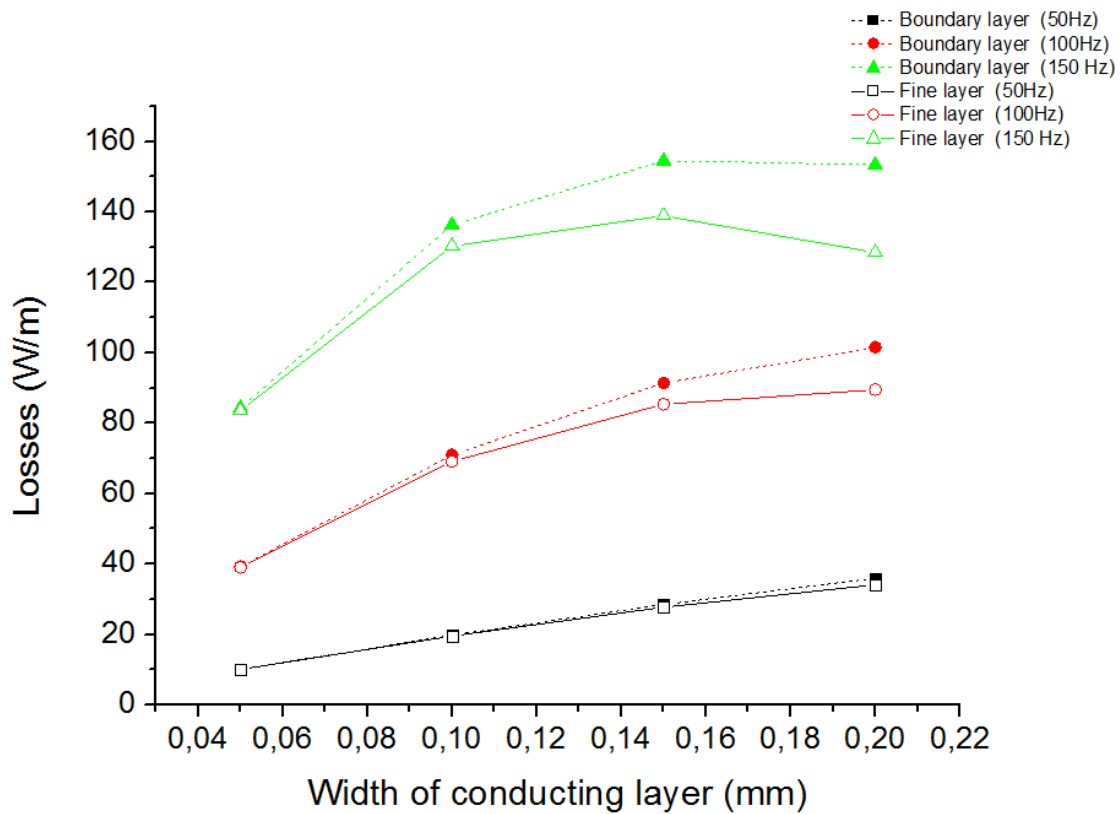


Figure 16: Comparison of losses between the boundary layer model and fine mesh model

3.5 Computation algorithm and incorporation in FCSMEK

The space discretization of the boundary layer model given by equation (3.38) was done by finite element method where potentials in each element are discretized by replacing weight function w , with shape functions of active nodes. In this case, it is assumed that the potential varies linearly and hence the shape function is a linear polynomial and 'finite element' is a first order triangular element. The application of a finite element method results to a system of equations as [38],

$$\mathbf{S} \mathbf{a} + \mathbf{T} \dot{\mathbf{a}} = 0 \quad (3.39)$$

where,

$$\begin{aligned} \mathbf{S}_{ij} &= \int_{\Omega} \nu \nabla N_i \cdot \nabla N_j d\Omega, \\ & i, j = 1, \dots, 3 \\ \dot{\mathbf{a}} &= \frac{\partial \mathbf{a}}{\partial t} \\ \mathbf{T}_{ij} &= \int_{\Gamma_{ia}} \sigma h N_i N_j d\Gamma, \\ & i, j = 1, \dots, 3 \end{aligned} \quad (3.40)$$

In air region, the system of equations is solved as $\nu = \nu_2$ (constant) and in non-linear material of insulated sheet, the equations are solved as $\nu = \nu_1(B^2)$ where reluctivity (ν_1) depends on the magnetic field at least at flux densities higher than 1 T [38]. The time dependent nodal value vector \mathbf{a} is time discretized by Crank-Nicolson method as explained in section 3.6. The non-linearity of the material was solved by Newton-Raphson method which corrects the nodal value of \mathbf{a} at each step as explained in section 3.7. It is important to note that \mathbf{T}_{ij} is line integration along the material boundaries and shape functions N_i and N_j correspond to only those nodes that belong to material boundaries.

The inhouse software FCSMEK has the system of equations similar to the matrix form as shown in equation (3.39). FCSMEK is a FORTRAN based software developed in Research Group of Electromechanics of Aalto University and is generally used to study 2-D finite element analysis of electrical machines based on magnetic vector potential. The incorporation of boundary layer model in FCSMEK can be done by firstly, identifying the boundary of the material where the model is to be implemented and secondly, by taking line integration along the boundary and forming \mathbf{T} matrix as shown in equation (3.40) then finally, adding it to the existing system of equations. The detailed procedure for finding the material boundary and of numerical integration is described as following.

3.5.1 Boundary identification

In FCSMEK, meshing of geometry (space discretization) can be done with linear, quadratic or cubic polynomials. Linear meshing results to three nodes per element as explained in section 3.1.1. Each element is assigned with a material index and boundary node and periodic ones are assigned with a boundary condition. The parameters including the dimensions of the geometry, its type of material and the supply characteristics are stored in *cim.data* file and once the geometry is meshed, the information about the coordinates of the nodes, number of elements, boundary conditions, index of the number of nodes per element, nodal values, material type of each element and all the required informations are stored in *cim.fedat* file.

The *cim.fedat* file was firstly studied in MATLAB and an algorithm to identify the material boundary was developed in MATLAB. The flow chart describing the identification of boundary between two materials is shown in Figure 17. To identify the material boundary in finite elements, the material index of each element was checked by looping over all the other elements and the element of different material was identified. Elements of two different materials are separated by common edge as shown in Figure 21b. The nodes at the common edges were found by looping over the nodes of identified elements. The identified element and nodes of material boundary were assigned with index and stored in matrix which is used later in numerical integration. The same algorithm is then implemented in FCSMEK to identify the material boundary for UI sheets and induction machine. The identified material boundary from FCSMEK was plotted in MATLAB and shown in Figure 23b.

3.5.2 Incorporation in FCSMEK

FCSMEK has collection of routines which are used in preprocessing, FEM analysis and postprocessing. The preprocessing routine is MESH which is used to space discretize the geometry. SYDC, CIMAC and CIMTD are the routines which are used to do finite element analysis. CIMAC calculates initial values by doing time harmonic calculation. CIMTD does the time stepping analysis and solves circuit equations. CIMPLOT is the post processing routine which is used to plot the solutions. The flow of programs in computing field solution for induction machine in FCSMEK is attached in Appendix. The incorporation of boundary layer model is done in CIMTD module. The discretization of field equations, circuit equations and formation of coefficient matrix for SPARSPAK solvers are formed in CIMTD module. The boundary layer model due to conducting edges as explained in section 3.3 is added to the system of non-conducting irons equations (3.39) of *trtd* routine in CIMTD. The \mathbf{T} comprises the line integration of the boundary line and the numerical integration procedure for boundary line is explained in the following section.

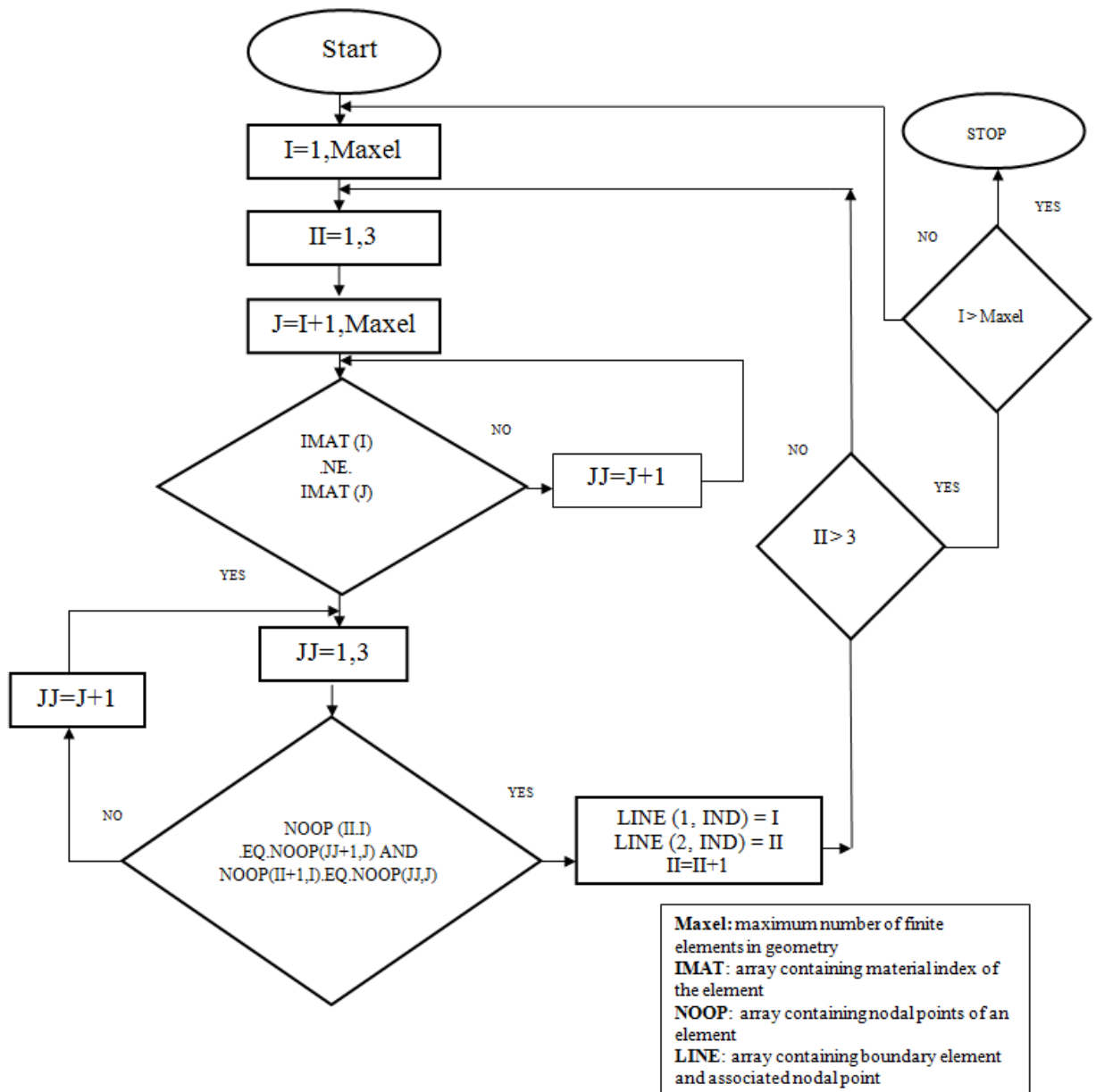


Figure 17: Flowchart for identifying boundary line of an element of different material

3.5.3 Numerical integration

The solution of equations (3.39),(3.40) and computation of losses along the boundary line requires numerical integration. The Gaussian quadrature method was applied to perform the numerical integration. In the finite element application, the integral of function f over a triangular element can be evaluated as summation of the product of function at each integration points, weighting function for each point and the determinant of the Jacobian matrix at each point. The mathematical expression is shown in equation (3.41).

The multiplication by determinant of Jacobian matrix does the coordinate transformation from reference $u-v$ plane to global $x-y$ plane. In case of triangular element, the determinant of the Jacobian matrix is twice the area of the triangle. The integration along the edge of the first order triangular element involves two nodal points and the determinant of the Jacobian matrix is the length of the line defined by the two nodal points. The minimum number of required integration points for integrating along the edge is one but during the integration of \mathbf{T} matrix in the boundary layer model, the product of two shape function varies quadratically and hence two integration points were considered.

The potential variation of first order triangular element and 1-D element is shown in Figure 18. The integration points and weight points are shown in Appendix.

$$\int_{\Omega} f(x, y) d\Omega = \frac{1}{2} \sum_{i=1}^n w_i f_i(u, v) |J_i| \quad (3.41)$$

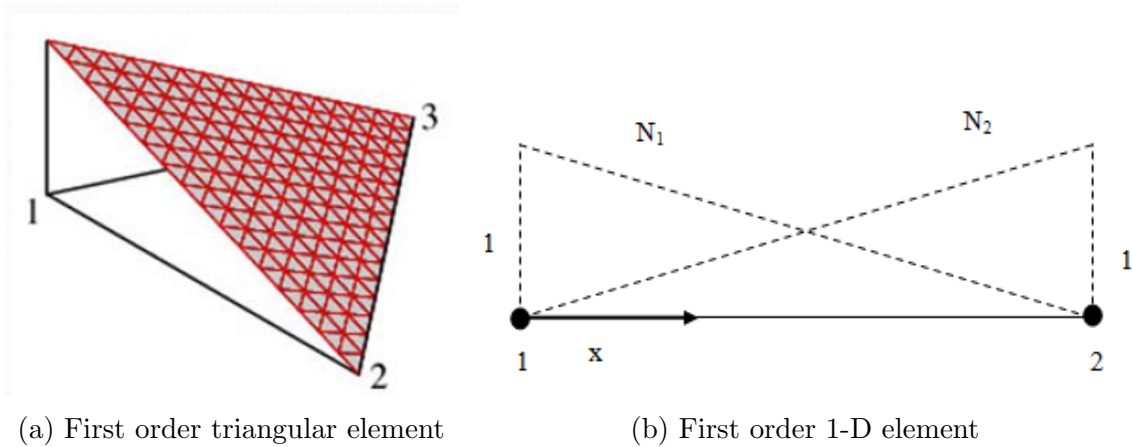


Figure 18: Potential variation in first order 2-D and 1-D element

4 Results and discussion

4.1 Boundary layer model implementation in UI sheets

The boundary layer model was incorporated into inhouse software FCSMEK and the solutions were compared with the solutions obtained from COMSOL MultiphysicsTM. The comparison was done on standard geometry of UI90 sheet where non-linear iron material STABOLEC 260-50A was used. The bh curve of the material is shown in Figure 19.

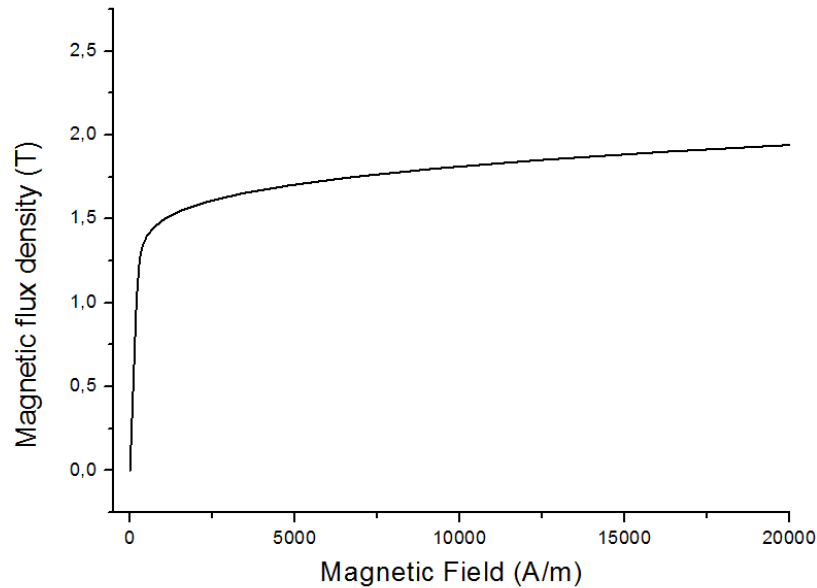
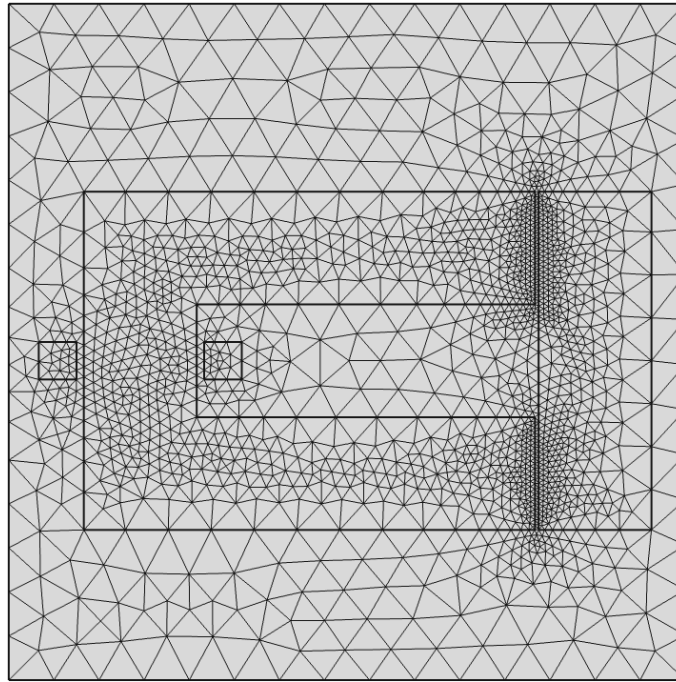
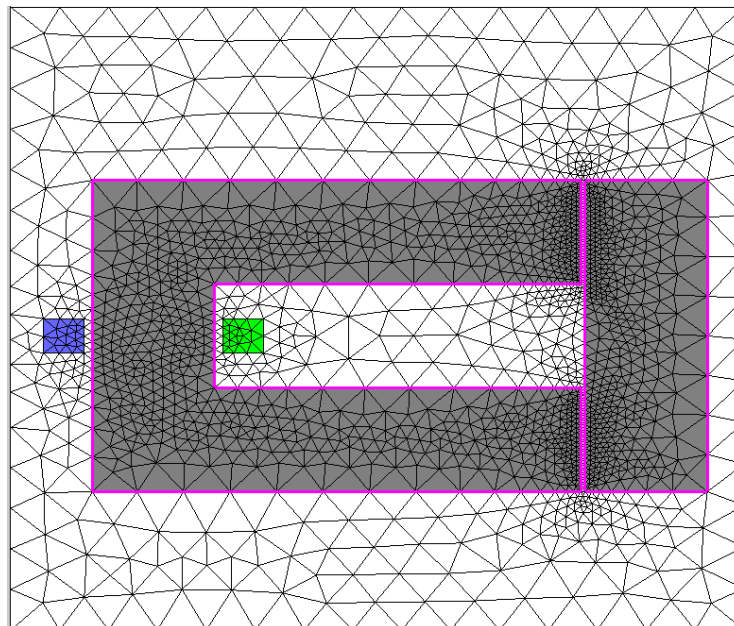


Figure 19: BH curve of STABOLEC 260-50A iron sheet.

The geometry of UI90 sheet was constructed in COMSOL MultiphysicsTM. It was meshed with 3348 linear triangular elements and the mesh from the COMSOL MultiphysicsTM was exported and used in FCSMEK. The exported mesh from COMSOL MultiphysicsTM was in Nastran format which is not compatible with FCSMEK so a MATLAB subroutine was used to parse the exported mesh from COMSOL to make it compatible with FCSMEK. The meshes obtained from the two softwares are shown in Figure 20. The boundary layer model was implemented in both the softwares considering the conductivity ($\sigma = 3 \text{ MS/m}$) and burr width ($h = 0.2 \text{ mm}$). The flux distributions at last time period obtained from the two softwares were plotted in Figure 21.

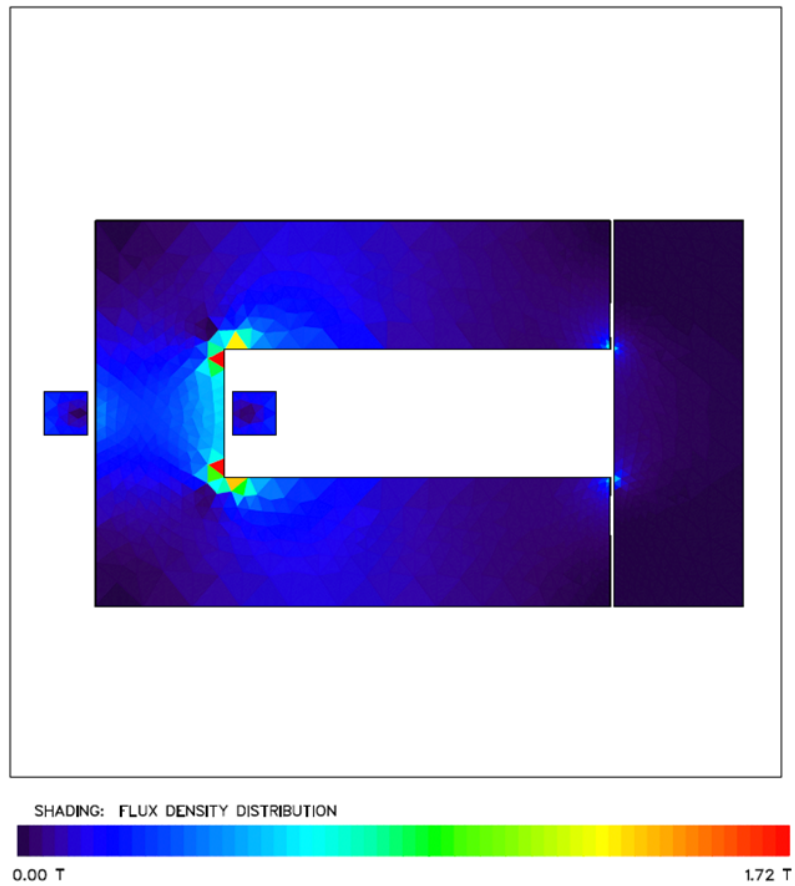


(a) Mesh obtained from COMSOL for UI90 sheet

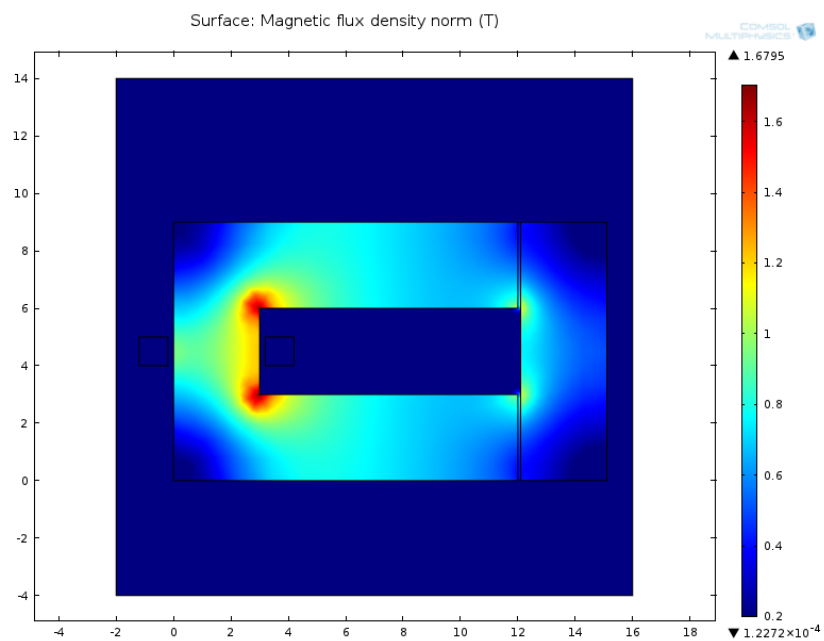


(b) Exported mesh from COMSOL used in FCSMEK

Figure 20: Transfer of mesh



(a) Flux density distribution at 3000 A at 60 ms in FCSMEK



(b) Flux density distribution at 3000 A at 60 ms in COMSOL

Figure 21: Comparison of flux density distribution

Time stepping analysis was done for 200 steps per period and three periods were studied for 50 Hz frequency. The non-linearity was solved by Newton-Raphson method and time discretization was done by using Crank-Nicolson method. The sinusoidal source current was supplied and the peak current was varied from 500 A to 5000 A and the losses were computed in both the models and compared as shown in Figure 22. The loss computation was done in the last time period in both the models and the loss was computed along the boundary line using

$$\int_{\Gamma} \sigma h \left(\frac{d\mathbf{A}}{dt} \right)^2 d\Gamma, \quad (4.1)$$

Equation 4.1 was numerically calculated considering two integration points as explained in section 3.5.3.

The losses computed from the two different softwares were similar. However, difference of less than 3 % was obtained in the computed loss which may be due to a numerical error in considering the integration points. Since, during loss computation, the integration points in both the software were not the same.

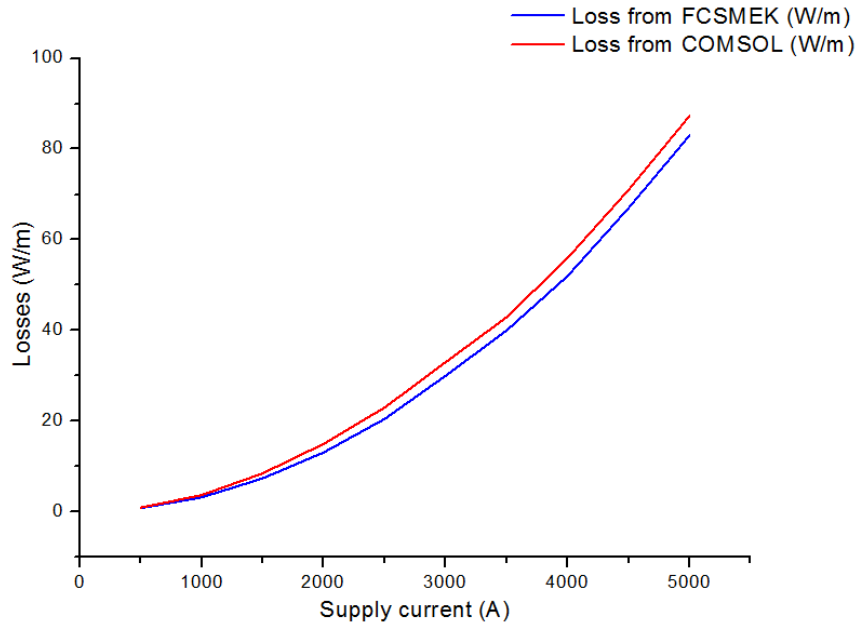
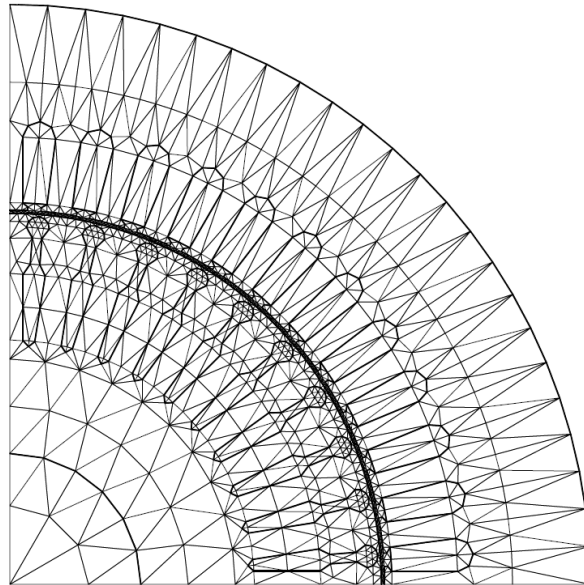


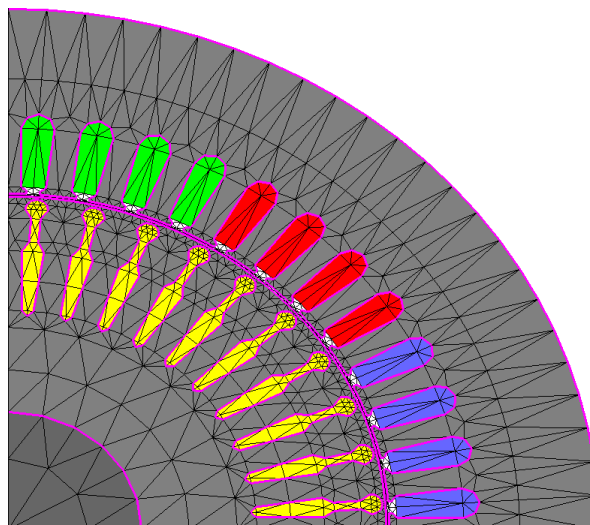
Figure 22: Comparison of losses obtained from FCSMEK and COMSOL

4.2 Model application in cage induction machine

The losses computed for UI sheets using the boundary layer formulation from inhouse software and COMSOL Multiphysics TM were similar. Moreover, the computation time in inhouse software was less compared to COMSOL Multiphysics TM. So, the 37 kW induction machine was studied implementing the boundary model in FC-SMEK. The cross section of the geometry and the identified boundary are shown in Figure 23a and Figure 23b, respectively.



(a) First order triangular element mesh for induction machine



(b) Material boundary identified where boundary layer model is implemented

Figure 23: Geometry of studied induction machine

The developed subroutine in FCSMEK was used to implement the boundary layer model. The end effect of the machine is neglected since the reduced scalar potential was not included in the boundary layer model. The model was studied with 1841 linear triangular elements. The material for the stator and rotor was STABOLEC 260-50A. The bh curve is shown in Figure 19. The non-linearity was solved by Newton-Raphson method. The Crank-Nicolson method as explained in section 3.1.2 was used for time discretization.

The machine parameters and the time stepping results obtained with and without the model is tabulated in Table 1. The boundary layer model with conductivity ($\sigma = 3\text{MS/m}$) and burr width $1\ \mu\text{m}$ slightly increases the terminal current and torque. This causes the slight increase in the resistive loss of the rotor and stator. The total stator loss was increased by 10 %. The difference between field solutions

| Machine parameters | With boundary layer model | Without the boundary layer model |
|-------------------------------|---------------------------|----------------------------------|
| Terminal voltage | 400 V | 400 V |
| Terminal current | 62.76 A | 61.6 A |
| Power factor | 0.797 | 0.8174 |
| Slip | 0.01 | 0.01 |
| Rotational speed | 1485 | 1485 |
| Air-gap torque | 219.201 Nm | 218.997 Nm |
| Shaft power | 34.09 kW | 34.06 kW |
| Air-gap flux density | 0.867 T | 0.872 T |
| Stator temperature | 50 C | 50 C |
| Resistive loss in st.winding | 859.48 W | 815.31 W |
| Core losses in the stator | 564.03 W | 564.53 W |
| Rotor temperature | 50 C | 50 C |
| Total resistive loss of rotor | 477.20 Nm | 476.39 Nm |
| Core losses in rotor | 200.44 W | 200.68 W |
| Total stator loss | 1423.51 W + 94.54 W | 1379.84 W |
| Rotor losses | 677.64 W | 677.84 W |
| Total electromagnetic loss | 2195.69 W | 2056.91 W |

Table 1: Results from time stepping analysis

obtained with and without the boundary layer model is shown in Figure 24. The losses were computed along the boundary edge at slip 0.01 over the last time period. The increase in the total electromagnetic losses due to inter-laminar contact at conductivity $3\ \text{MS/m}$ and burr width $1\ \mu\text{m}$ was 6.78%.

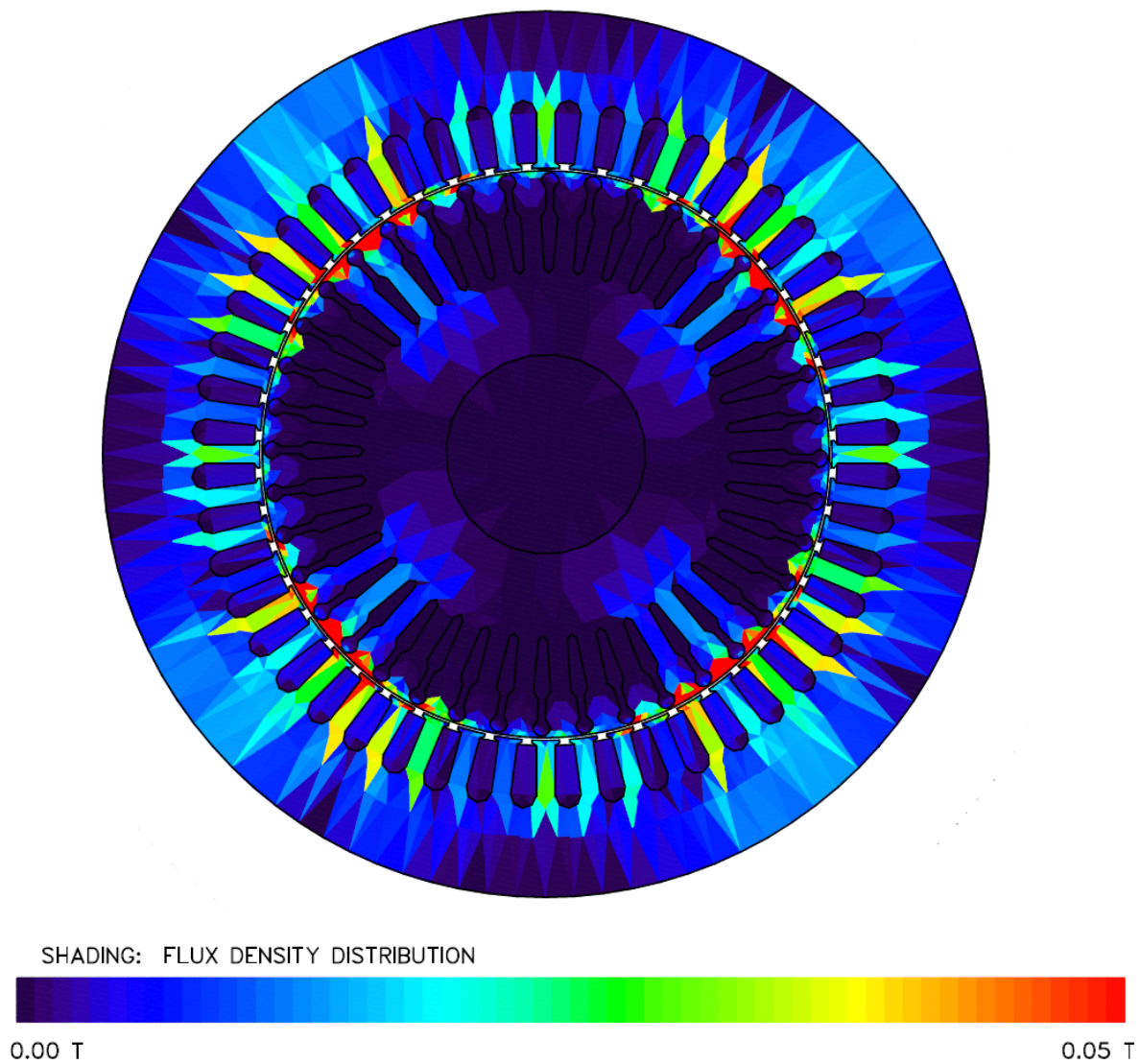


Figure 24: Difference of field solution

5 Conclusion

The burr formed at the edges of sheets during the punching deteriorates the insulation of adjacent sheets and forms the random inter-laminar galvanic contacts during stacking of the sheets. The bolts or the welding seam which is used to hold the sheets provides the path for eddy current and causes additional losses. The burred region is in range of few micrometers and hence to model this burred region using only finite elements requires very fine mesh and high computation time. So, a boundary layer model was developed and coupled to 2-D finite elements to model the additional losses in electrical machines due to inter-laminar galvanic contacts at the edges of electrical sheets. The boundary layer model does not require a fine mesh along the burred region. The boundary layer model was compared with a fine mesh model and it has acceptable accuracy at 50 Hz and at burr width less than 0.1 mm. The developed boundary layer model is incorporated into an inhouse software FCSMEK which is a FORTRAN based software. The coupled boundary layer model can be used to predict the additional loss caused by inter-laminar galvanic contacts at the edges of sheets. Prediction of such losses is essential for electric machines manufacturers. The losses introduced due to the manufacturing process which are still under study adds up the heat in the machine. The accurate prediction of such losses allows proper design and a cooling system which not only prevents the damage of the machine in future operations but also saves the cost of maintenance.

However, the formation of the burr is stochastic in nature and depends on the age of the punching tools and the galvanic contacts are random in nature. The randomness of the contacts can be incorporated into the developed model by identifying the conductivity distribution. The distribution of the conductivity can be obtained statistically by measuring conductivity of numerous samples of electrical sheets by varying the stacking pressure. The obtained distribution can later be validated by a statistical and stochastic approach.

The coupled boundary layer model is applicable to thin edges where the current density is assumed to be constant and the accuracy of the model can be improved by adding the skin effect conditions.

References

- [1] J. Barranger, “Hysteresis and eddy current losses of a transformer lamination viewed as an application of the Poynting theorem,” tech. rep., National Aeronautics and Space Administration, Lewis Research Center, Cleveland, Ohio, November, 1965.
- [2] G. Biorci and D. Pescetti, “Analytical theory of the behaviour of ferromagnetic materials,” *Nuovo Cimento*, vol. 7, pp. 829–842, 1958.
- [3] N. Burais, “Iron losses calculation in non-oriented steel plate,” *IEEE Transactions on Magnetics*, vol. 17, pp. 2577 – 2579, nov 1981.
- [4] N. Burais and G. Grellet, “Numerical modelling of iron losses in ferromagnetic steel plate,” *IEEE Transactions on Magnetics*, vol. 18, pp. 558 – 562, mar 1982.
- [5] D. Jiles and D. Atherton, “Theory of ferromagnetic hysteresis,” *Journal of Magnetism and Magnetic Materials*, vol. 61, no. 12, pp. 48 – 60, 1986.
- [6] J. P. A. Bastos and N. Sadowski, *Electromagnetic Modeling by Finite Element Methods*. CRC Press, 1 ed., 2003.
- [7] G. Bertotti, “Physical interpretation of eddy current losses in ferromagnetic materials. i. theoretical considerations,” *Journal of Applied Physics*, vol. 57, no. 6, pp. 2110–2117, 1985.
- [8] W. Arshad, T. Ryckebusch, F. Magnussen, H. Lendenmann, B. Eriksson, J. Soulard, and B. Malmros, “Incorporating lamination processing and component manufacturing in electrical machine design tools,” in *Industry Applications Conference, 2007. 42nd IAS Annual Meeting. Conference Record of the 2007 IEEE*, pp. 94 –102, sept. 2007.
- [9] P. Baudouin, M. D. Wulf, L. Kestens, and Y. Houbaert, “The effect of the guillotine clearance on the magnetic properties of electrical steels,” *Journal of Magnetism and Magnetic Materials*, vol. 256, no. 13, pp. 32 – 40, 2003.
- [10] F. Ossart, E. Hug, O. Hubert, C. Buvat, and R. Billardon, “Effect of punching on electrical steels: Experimental and numerical coupled analysis,” *IEEE Transactions on Magnetics*, vol. 36, pp. 3137 –3140, sep 2000.
- [11] A. Kedous-Lebouc, B. Cornut, J. Perrier, P. Manfé, and T. Chevalier, “Punching influence on magnetic properties of the stator teeth of an induction motor,” *Journal of Magnetism and Magnetic Materials*, vol. 254255, pp. 124 – 126, 2003. Proceedings of the 15th International Conference on Soft Magnetic Materials (SMM15).
- [12] A. Boglietti, A. Cavagnino, L. Ferraris, and M. Lazzari, “The annealing influence onto the magnetic and energetic properties in soft magnetic material after punching process,” in *IEEE Electric Machines and Drives conference*, (Wisconsin, USA), June 2003.

- [13] S. B. Lee, G. Kliman, M. Shah, W. Mall, N. Nair, and R. Lusted, “An advanced technique for detecting inter-laminar stator core faults in large electric machines,” *IEEE Transactions on Industry Applications*, vol. 41, pp. 1185 – 1193, sept.-oct. 2005.
- [14] S. J., “Theory of electromagnetic testing of laminated stator cores,” *Insight (Northampton)*, vol. 36, no. 4, pp. 246–251, 1994. eng.
- [15] R. Jean-Yves, V. Emmanuel, H. Thomas, B. Abdelkader, and D. Jean-Pierre, “Electromagnetic modelling of short circuited coreplates,” *COMPEL: The International Journal for Computation and Mathematics in Electrical and Electronic Engineering*, vol. 28, pp. 762–771, 2009.
- [16] D. M. Lindenmo, A. Coombs, “Advantages, properties and types of coatings on non-oriented electrical steels,” *Journal of Magnetism and Magnetic Materials*, vol. 215-216, pp. 79–82, 2000.
- [17] M. Emura, F. Landgraf, W. Ross, and J. Barreta, “The influence of cutting technique on the magnetic properties of electrical steels,” *Journal of Magnetism and Magnetic Materials*, vol. 254255, pp. 358 – 360, 2003.
- [18] A. Schoppa, J. Schneider, and J.-O. Roth, “Influence of the cutting process on the magnetic properties of non-oriented electrical steels,” *Journal of Magnetism and Magnetic Materials*, vol. 215216, pp. 100 – 102, 2000.
- [19] K. Schmidt, “Influence of punching on the magnetic properties of electric steel with 1 percent silicon,” *Journal of Magnetism and Magnetic Materials*, vol. 2, Issue 1-3, pp. 136–150, December 1975.
- [20] A. Moses, N. Derebasi, G. Loisos, and A. Schoppa, “Aspects of the cut-edge effect stress on the power loss and flux density distribution in electrical steel sheets,” *Journal of Magnetism and Magnetic Materials*, vol. 215 - 216, pp. 690 – 692, 2000.
- [21] P.Beckley, *Electrical Steels for Rotating Machines*. The Institution of Engineering and Technology, London, 2002.
- [22] D. D. Ko SL, “A study on burr formation mechanism,” *Transaction of the ASME Journal of Engineering Materials and Technology*, vol. 113(1), pp. 75–87, 1991.
- [23] ISO13715:2000, “Technical drawings-edges of undefined shape-vocabulary and indications.”
- [24] L. K. Gillespie and P. T. Blotter, “The formation and properties of machining burrs,” *Journal of Engineering for Industry*, vol. 98, no. 1, pp. 66–74, 1976.
- [25] J. Aurich, D. Dornfeld, P. Arrazola, V. Franke, L. Leitz, and S. Min, “Burrs-analysis, control and removal,” *CIRP Annals - Manufacturing Technology*, vol. 58, no. 2, pp. 519 – 542, 2009.

- [26] R. Mazurek, H. Hamzehbahmani, A. Moses, P. Anderson, F. Anayi, and T. Belgrand, “Effect of artificial burrs on local power loss in a three-phase transformer core,” *IEEE Transactions on Magnetics*, vol. 48, pp. 1653–1656, april 2012.
- [27] C. A. Schulz, S. Duchesne, D. Roger, and J.-N. Vincent, “Capacitive short circuit detection in transformer core laminations,” *Journal of Magnetism and Magnetic Materials*, vol. 320, no. 20, pp. 911–914, 2008. Proceedings of the 18th International Symposium on Soft Magnetic Materials.
- [28] R. Mazurek, P. Marketos, A. Moses, and J.-N. Vincent, “Effect of artificial burrs on the total power loss of a three-phase transformer core,” *IEEE Transactions on Magnetics*, vol. 46, pp. 638–641, feb. 2010.
- [29] A. Moses and M. Aimoniotis, “Effects of artificial edge burrs on the properties of a model transformer core,” *Physica Scripta*, vol. 39, pp. 391–393, 1989.
- [30] J. Van der Veen, L. Offringa, and A. Vandenput, “Minimising rotor losses in high-speed high-power permanent magnet synchronous generators with rectifier load,” *IEE Proceedings - Electric Power Applications*, vol. 144, pp. 331–337, sep 1997.
- [31] Igarashi, H., Kost, A., and Honma, T., “Impedance boundary condition for vector potentials on thin layers and its application to integral equations*,” *The European Physical Journal Applied Physics*, vol. 1, no. 1, pp. 103–109, 1998.
- [32] C. Brebbia, *Topics in Boundary Element research*. Springer-Verlag Berlin, Heidelberg, 1989.
- [33] L. Krahenbuhl and D. Muller, “Thin layers in electrical engineering-example of shell models in analysing eddy-currents by boundary and finite element methods,” *IEEE Transactions on Magnetics*, vol. 29, pp. 1450–1455, mar 1993.
- [34] C. Geuzaine, P. Dular, and W. Legros, “Dual formulations for the modeling of thin electromagnetic shells using edge elements,” *IEEE Transactions on Magnetics*, vol. 36, pp. 799–803, jul 2000.
- [35] J. Gyselinck, R. Sabariego, P. Dular, and C. Geuzaine, “Time-domain finite-element modeling of thin electromagnetic shells,” *IEEE Transactions on Magnetics*, vol. 44, pp. 742–745, june 2008.
- [36] R. Sabariego, C. Geuzaine, P. Dular, and J. Gyselinck, “Nonlinear time-domain finite-element modeling of thin electromagnetic shells,” *IEEE Transactions on Magnetics*, vol. 45, pp. 976–979, march 2009.
- [37] A. Leissa, “The historical bases of the rayleigh and ritz methods,” *Journal of Sound and Vibration*, vol. 287, no. 45, pp. 961–978, 2005.
- [38] J. Luomi, “Finite element methods for electrical machines.” Chalmers University of Technology, Department of Electrical Machines and Power electronics, Goteborg, 1993. Lecture notes.

APPENDIX A

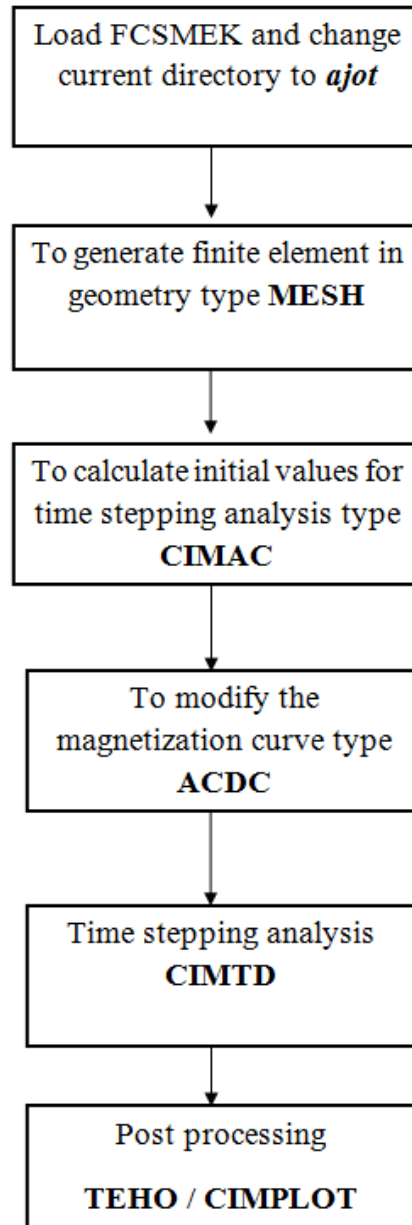


Figure 25: Flow of command line in Time step analysis of induction machine in FCSMEK

APPENDIX B

Gaussian quadrature rule

A gaussian quadrature rule is a method to calculate definite integral of function numerically. It is done by taking weighted sum of function at specified points within the domain of integration. A polynomial of $2m-1$ can be calculated using m number of integration points. The weight values and integration points for different order of polynomials are tabulated below.

| m | x_i | weight W_i |
|---|----------------|--------------|
| 1 | 0 | 2 |
| 2 | ± 0.5777 | 1 |
| 3 | 0 | 0.88889 |
| | ± 0.7745 | 0.555556 |
| 4 | ± 0.339981 | 0.652145 |
| | ± 0.861136 | 0.347855 |
| 5 | 0 | 0.568889 |
| | ± 0.538469 | 0.478629 |
| | ± 0.90618 | 0.236927 |